Equilibrium Partial Pressures, Thermodynamic Properties of Aqueous and Solid Phases, and Cl_2 Production from Aqueous HCl and HNO_3 and Their Mixtures

Mario Massucci, Simon L. Clegg,* and Peter Brimblecombe

School of Environmental Sciences, University of East Anglia, Norwich NR4 7TJ, U.K.

Received: December 10, 1998; In Final Form: February 22, 1999

Equilibrium total pressures have been measured above aqueous HNO_3 (for 7.82, 15.73, and 35.99 mol kg^{-1} solutions from 294.6 to 224.7 K) and aqueous HCl (9.45 and 10.51 mol kg^{-1}, from 289.4 to 199.5 K) using a capacitance manometer. Equilibrium partial pressures of the acids have also been determined, by mass spectrometry, from 274.8 to 234.6 K for both HCl solutions, and from 265.0 to 240.1 K for 15.73 mol kg^{-1} HNO_3. Results are generally consistent with model predictions, though with small (∼10%) systematic deviations for the total pressure measurements over aqueous HCl at about 220 K. Mixtures of $HCl-HNO_3-H_2O$ composition yielded measured total pressures orders of magnitude greater than predicted for the gases H_2O, HNO_3, and HCl. Mass spectrometric determinations and equilibrium thermodynamic calculations suggest that Cl_2 and NOCl were produced by the reaction: $4H^+_{(aq)} + NO_3^-{}_{(aq)} + 3Cl^-_{(aq)} \rightleftharpoons NOCl_{(aq)} + Cl_{2(aq)} + 2H_2O_{(l)}$, which is known to occur in aqua regia (a mixture of concentrated hydrochloric and nitric acids). Calculations for aqueous solutions of stratospheric aerosol composition suggest, purely on equilibrium grounds (and neglecting kinetics), that the reaction could be a source of active chlorine in the stratosphere. The correlation of Clegg and Brimblecombe (*J. Phys. Chem.* **1990**, *94*, 5369−5380; and **1994**, *96*, 6854) of the thermodynamic properties of aqueous HNO_3 activities has been revised, and vapor pressure products (for the reaction $HNO_3{\cdot}nH_2O_{(cr)} \rightleftharpoons HNO_{3(g)} + nH_2O_{(g)}$, where $1 \le n \le 3$) assessed from literature studies. The activity product for the reaction $HNO_3{\cdot}2H_2O_{(cr)} \rightleftharpoons H^+_{(aq)} + NO_3^-{}_{(aq)} + 2H_2O_{(l)}$ has also been determined. The model of Carslaw et al. (*J. Phys. Chem.* **1995**, *99*, 11557−11574) has been revised for the solubility of HBr in aqueous H_2SO_4 to stratospheric temperatures.

1. Introduction

Predicting the behavior of stratospheric aerosols at low temperature requires a knowledge of the thermodynamic properties of $H_2SO_4-HNO_3-H_2O$ mixtures, including the solubilities of trace gases such as HCl and HBr. These gases are important because they react with other species on aerosol droplets or particles to produce active Cl_2 and Br_2.[1]

A thermodynamic model of the system has been developed by Carslaw et al.,[2] based upon measurements for the pure aqueous acids and their mixtures. The data at low temperatures are extensive for aqueous HNO_3,[3] and especially H_2SO_4,[4] but are largely restricted to ≥273.15 K for aqueous HCl and HBr.[2] The mixed system $H_2SO_4-HNO_3-H_2O$ has been relatively well studied at stratospheric temperatures (see Table 11 of Carslaw et al.[2]), but measurements of HBr solubilities in aqueous H_2SO_4, and of HCl in ternary $H_2SO_4-HNO_3-H_2O$ mixtures, have been sparse until recently.

In this study we have measured total and partial pressures above $HCl-H_2O$ and HNO_3-H_2O to 199.5 K to improve our understanding of their behavior. The results are presented here and compared with predictions of the model of Carslaw et al.[2]

Experiments were also carried out to determine equilibrium and total pressures above $HCl-HNO_3-H_2O$ solutions for $203.3 \le T \le 264.8$ K. Chlorine and, it is thought, NOCl were produced in significant quantities in the solutions, probably by the reaction long known to occur in aqua regia,[5] the highly concentrated mixture of hydrochloric and nitric acids. The results for this system are compared with partial pressures calculated from available thermodynamic data, and the implications for production of Cl_2 in aqueous stratospheric aerosols are explored.

We have also determined equilibrium constants for the formation of the solid $HNO_3{\cdot}2H_2O_{(cr)}$, and the partial pressure products $pHNO_3pH_2O^n$ over nitric acid hydrates $HNO_3{\cdot}nH_2O$ ($1 \le n \le 3$), based upon currently available measurements. The model of Carslaw et al.[2] has been revised for HBr solubilities in aqueous H_2SO_4, and predicted equilibrium partial pressures of HCl above $HCl-HNO_3-H_2SO_4-H_2O$ mixtures have been compared with recent literature data.

2. Theory

2.1. Equations. The solubility of an acid gas HX in an aqueous solution is here represented by the reaction:

$$HX_{(g)} \rightleftharpoons H^+_{(aq)} + X^-_{(aq)} \tag{1}$$

$$^xK_H(HX) = a_H a_X / pHX = x_H f_H{}^* x_X f_X{}^* / pHX \tag{2}$$

where $^xK_H(HX)$ (atm^{-1}) is the Henry's law constant, a_i is the activity of ion i, and pHX (atm) is the equilibrium partial pressure of HX. Aqueous phase activities are expressed on a mole fraction basis, thus x_i is the mole fraction of species i, and f_i* is its activity coefficient (with a reference state of infinite dilution with respect to the solvent, water). Expressions for calculating x_i and activity coefficients f_i* are given by Clegg et al.[6] and by Carslaw et al.[2] for the mixed acid solutions being studied here.

10.1021/jp9847179 CCC: $18.00
Published on Web 05/12/1999

Solid−liquid equilibrium is represented by the reaction

$$M_{\nu+}X_{\nu-}\cdot nH_2O_{(cr)} \rightleftharpoons \nu_+M^{x+}_{(aq)} + \nu_-X^{y-}_{(aq)} + nH_2O_{(l)} \quad (3)$$

$$^xK_S(M_{\nu+}X_{\nu-}\cdot nH_2O) = a_M{}^{\nu+}\, a_X{}^{\nu-}\, a_{H_2O}{}^n = x_M{}^{\nu+} f_M{}^{*\nu+}\, x_X{}^{\nu-} f_X{}^{*\nu-}\, a_{H_2O}{}^n \quad (4)$$

where ^xK_S is the equilibrium constant for the dissolution of solid $M_{\nu+}X_{\nu-}\cdot nH_2O$, and is equal to the activity product of the ions and solvent in a solution saturated with respect to the solid.

Solid−gas equilibria for acids ($HX_{(cr)}$) and their hydrates ($HX\cdot nH_2O_{(cr)}$) are given by

$$HX\cdot nH_2O_{(cr)} \rightleftharpoons HX_{(g)} + nH_2O_{(g)} \quad (5)$$

$$K_P = pHX\; pH_2O^n \quad (6)$$

where K_P (atm^{n+1}) is the equilibrium pressure product over the solid. It is related to the solubility and Henry's law constants by the following expression:

$$K_P = (^xK_S/{}^xK_H)\cdot(pH_2O^\circ)^n \quad (7)$$

where pH_2O° (atm) is the vapor pressure of pure water at the temperature of interest.

The general expression for an equilibrium constant K as a function of temperature is given below:

$$\begin{aligned}\ln(K_{(T)}) = \ln(K_{(Tr)}) &+ (\Delta_rH^\circ/R)(1/T_r - 1/T)\\ &+ (\Delta a/R)(T_r/T - 1 + \ln(T/T_r))\\ &+ (\Delta b/2R)(T_r(T_r/T - 1) + T - T_r)\\ &+ (\Delta c/6R)(2T_r{}^2(T_r/T - 1) + T^2 - T_r{}^2)\\ &+ (\Delta d/12R)(3T_r{}^3(T_r/T - 1) + T^3 - T_r{}^3)\\ &+ (\Delta e/3.75R)(1.5T_r{}^{1.5}(T_r/T - 1) + T^{1.5} - T_r{}^{1.5})\end{aligned} \quad (8)$$

where T (K) is the temperature of interest, T_r (K) is a reference temperature, Δ_rH° (J mol^{-1}) is the enthalpy change for the reaction at the reference temperature, and R (8.3144 J mol^{-1} K^{-1}) is the gas constant. Equation 8 implies that the heat capacity change for the reaction, Δ_rC_p (J mol^{-1} K^{-1}), is given by the function $\Delta_rC_p = \Delta a + \Delta bT + \Delta cT^2 + \Delta dT^3 + \Delta eT^{3/2}$.

2.2. Thermodynamic Model. The model of Carslaw et al.[2] is used in this study to calculate aqueous phase activity coefficients f_i*, and solid formation and equilibrium acid gas partial pressures using the equations given above. Recent experimental studies of low-temperature equilibria involving aqueous solutions of the acids H_2SO_4, HNO_3, HCl, and HBr have increased the amount of data compared to that available at the time the model of Carslaw et al.[2] was developed. Based upon such studies, several different equations also now exist for stratospherically important quantities such as equilibrium partial pressure products above solid acid hydrates. In Appendix I we first of all revise the correlation of Clegg and Brimblecombe[3] (used by Carslaw et al.[2]) for activities of water and HNO_3 in pure aqueous nitric acid. In Appendix II, data for equilibrium partial pressures above three HNO_3 hydrates are critically compared, and new equations are presented. Formation of the solid $HNO_3\cdot 2H_2O_{(cr)}$ is also included in the model of Carslaw et al.[2] (Appendix II), and the model is comprehensively revised for solubilities of HBr in aqueous H_2SO_4 in Appendix III.

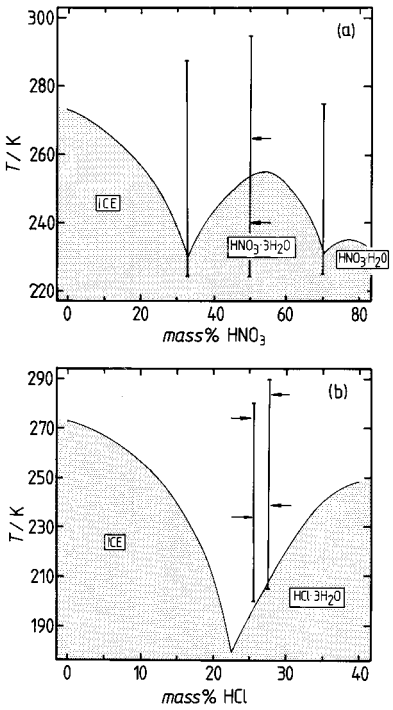

Figure 1. Temperatures (T) for which equilibrium pressures were measured for each of the test solutions. (a) Aqueous HNO_3. (b) Aqueous HCl. Vertical lines show the range of measurement of total pressure for each composition, and horizontal arrows indicate the smaller range of temperatures over which the partial pressures of the acid vapor were determined (three compositions only). The saturation curves with respect to ice and the acid hydrates are also shown.

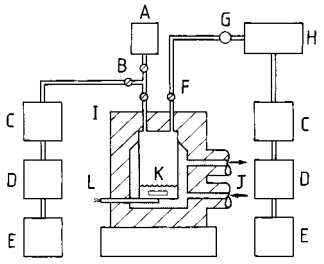

Figure 2. Schematic diagram of the apparatus: (A) capacitance manometers (only one shown), (B) connections to the vacuum line, (C) liquid nitrogen cooled trap, (D) diffusion pump, (E) rotary pump, (F) inlet for test solutions and connection to quadrupole mass spectrometer, (G) fine control needle valve, (H) differentially pumped quadrupole mass spectrometer, (I) thermally insulated test cell, (J) connections to refrigeration unit, (K) magnetically stirred test solution, (L) platinum resistance thermometer.

3. Experiments

Equilibrium pressures were measured over aqueous HNO_3 and aqueous HCl test solutions by capacitance manometer, using the method described by Massucci et al.[7] A modification to the apparatus enabled the composition of the vapor to be determined using a quadrupole mass spectrometer. The compositions and temperature ranges measured are shown in Figure 1, superimposed on the phase diagrams of the two acids.

3.1. Apparatus. The experimental setup is shown in Figure 2 and consists of a twin walled glass cell connected to a vacuum line, thermostatic bath, pressure gauges, and a quadrupole mass spectrometer. Total vapor pressures were measured using a pair

of capacitance manometers (Edwards Barocell model 655) covering the ranges $10-0.001$ and $0.1-10^{-5}$ Torr. Both were internally heated to 45 °C to minimize the effects of fluctuations of ambient temperature on the measurement of pressure and to ensure that vapors did not condense within the gauges.

The contents of the cell were degassed using a rotary and a diffusion pump, protected by a liquid nitrogen filled cold trap, capable of evacuating the vacuum line to 10^{-6} Torr. The temperature of the solution in the cell was controlled by passing ethanol from a refrigeration unit (Julabo F81 bath and VC circulator) between the cell walls. Temperature was controlled to a precision of ±0.025 K. The temperature of the cell was monitored by a platinum resistance probe mounted between the cell walls, in contact with the inner wall.

The capacitance manometers and thermometers monitoring the cell and the refrigeration unit were connected to a personal computer via a 16 bit A/D converter (Pico Technology ADC-16). Measurements were recorded at 1 min intervals. The A/D converter was operated at 14 bit resolution when recording temperature, resulting in a indicated resolution of 0.015 K. A higher resolution (16 bits) was used for recording the outputs from the manometers so that pressure measurements could be resolved to 0.015% of the full scale reading in each case. Corrections for thermal transpiration were made.

The composition of the vapor in the cell was analyzed using a quadrupole mass spectrometer (Vacuum Generators Spectralab 200D) pumped down below the 10^{-4} Torr threshold operating pressure using a rotary and a diffusion pump. A liquid nitrogen filled trap was used to protect the spectrometer from pump oils. The vapors were sampled through a glass capillary tube via a fine control needle valve. The sampling rate was kept low so as not to disturb the static equilibrium within the cell. Mass spectra were recorded at one minute intervals on the PC which controlled the operation of the mass spectrometer.

3.2. Materials. Aqueous HNO_3 test solutions were prepared from 69 mass % acid stock (BDH, Aristar grade) diluted with distilled water. Similarly, HCl test solutions were prepared from 35 mass % acid stock (BDH, Aristar grade). The molalities of the acid solutions were determined, before and after each experiment, by titration against aqueous sodium hydroxide (Aldrich Volumetric Standard). The uncertainty in the molality of each test solution was better than ±0.02 mol kg^{-1}.

The test solution containing 15.70 mol kg^{-1} HNO_3 and 2.15 mol kg^{-1} HCl was prepared as follows. Starting with the 15.73 mol kg^{-1} HNO_3 test solution in the cell from the previous experiment, weighed amounts of 69 mass % HNO_3 stock solution followed by 35 mass % HCl stock solution were transferred into the cell. Aliqots of test solution in the cell were titrated against aqueous NaOH volumetric standards after each addition of acid to ensure that the molalities matched calculated values.

3.3. Procedure. A 50 cm^3 aliquot of freshly prepared acid solution was transferred into the cell at room temperature and then cooled to 200 K. The cell was then opened to the vacuum line and the solution was degassed slowly to prevent explosive release of dissolved air. The cell was then warmed to room temperature and the cycle of cooling, evacuating, and warming was repeated until there were no changes in the observed vapor pressure at low temperature over several cycles, ensuring that the solution was air free.

Following degassing, the total vapor pressure of the magnetically stirred solution was measured. After the temperature of the refrigeration unit was set and the temperature in the cell had stabilized, the stopcocks between the cell and the capacitance manometers were opened. The vapor pressure in the cell was allowed to stabilize. Values of temperature and pressure were continuously recorded on the PC. Using 5 or 10 K steps, temperature equilibration was achieved in approximately 1 h, except at the lowest temperatures where the response of the refrigeration unit was slowest. Stabilization of the vapor pressure took about 2 h, after which the temperature was reset. The onset of freezing of the solution was monitored visually through a removable section of the thermal insulation enclosing the cell.

Partial pressures of HNO_3 and HCl were determined over solutions of 15.73 mol kg^{-1} HNO_3, and 9.45 mol kg^{-1} and 10.51 mol kg^{-1} HCl, respectively. After a series of total pressure measurements were made, the stopcock to the capillary line to the mass spectrometer was opened and the vapor in the cell was sampled though the needle valve. Mass spectra fragments due to water (for the main peak at $m/z = 18$ for H_2O^+) and HNO_3 (at $m/z = 30$ for the NO^+ fragment) or HCl (at $m/z = 36$ for the main peak for HCl^+) were recorded at 1 min intervals for between 30 and 100 min. Expected peaks for HNO_3 at $m/z = 63$ (due to HNO_3^+) and $m/z = 46$ (due to NO_2^+) were unresolved. The minor peaks for HCl at $m/z = 38$, 35, and 37, in order of relative signal size, were observed and recorded but not used in the determination of HCl partial pressure. The needle valve was then opened further and another series of signals were recorded. This was repeated until the pressure in the mass spectrometer approached the threshold operating pressure or when the needle valve was fully open. A plot was then made of the signal due to HNO_3 or HCl relative to that of H_2O, and $pHNO_3$ or pHCl were calculated using the equilibrium pH_2O predicted by the model of Carslaw et al.[2] as the reference.[8]

Only a few measurements were made on the vapor above the $HCl-HNO_3-H_2O$ mixture, not under equilibrium conditions, to avoid corrosion damage to the equipment that might be caused by the relatively high pressures encountered. For chlorine species the mass spectrum was again recorded for peaks $m/z = 35-38$, but instead of the four peaks previously seen for HCl in this region only two peaks were observed, at $m/z = 35$ (major peak) and 37 (minor peak). Two smaller peaks, which were not present in the earlier experiments on pure aqueous HCl, were also noted at $m/z = 70$ and 72. It was concluded from these observations, and calculations of the equilibrium state of the system (section 4.3), that the spectrum observed was due to Cl_2 and the signal for the major peak at $m/z = 35$ was therefore used to calculate pCl_2.

The NO^+ peak at $m/z = 30$ was found to be many times higher than predicted for HNO_3, and our calculations (section 4.3) suggest that NOCl has a partial pressure higher than the other N-containing species in the system by about 2 orders of magnitude. The signal at $m/z = 30$ was therefore used to calculate pNOCl, and not $pHNO_3$ as it was for the HNO_3-H_2O system. (Note that in the determination of pCl_2 a fraction of this signal was subtracted from the peak at $m/z = 35$ to account for the Cl^+ fragment arising from NOCl.)

4. Results

The measured total and partial pressures above HNO_3-H_2O and $HCl-H_2O$ solutions are listed in Tables 1−3. The results for the $HCl-HNO_3-H_2O$ mixture are not tabulated, but are discussed in section 4.3.

4.1. HNO_3-H_2O. Equilibrium total pressures ($pH_2O + pHNO_3$, from Table 1) above 7.82, 15.73, and 35.99 mol kg^{-1} $HNO_{3(aq)}$ are compared with predictions of the model of Carslaw et al.[2] in Figure 3. The inset to Figure 3a shows the calculated partial pressure fraction of HNO_3 in the gas phase, and indicates

TABLE 1: Equilibrium Total Pressures ($pH_2O + pHNO_3$) above Aqueous HNO_3 Solutions[a]

$mHNO_3$ (mol kg^{-1})	T (K)	P (atm)	$mHNO_3$ (mol kg^{-1})	T (K)	P (atm)	$mHNO_3$ (mol kg^{-1})	T (K)	P (atm)
7.82	287.6	1.15×10^{-2}	15.73	294.6	1.16×10^{-2}	35.99	275.1	1.78×10^{-3}
7.82	286.6	1.12×10^{-2}	15.73	291.9	9.66×10^{-3}	35.99	275.0	1.86×10^{-3}
7.82	284.7	9.70×10^{-3}	15.73	291.9	9.50×10^{-3}	35.99	275.0	1.88×10^{-3}
7.82	284.6	9.84×10^{-3}	15.73	289.6	8.18×10^{-3}	35.99	274.9	1.91×10^{-3}
7.82	284.4	9.60×10^{-3}	15.73	289.6	8.19×10^{-3}	35.99	274.9	1.90×10^{-3}
7.82	279.8	6.94×10^{-3}	15.73	289.4	7.79×10^{-3}	35.99	274.8	1.80×10^{-3}
7.82	279.5	6.90×10^{-3}	15.73	284.6	5.93×10^{-3}	35.99	269.9	1.17×10^{-3}
7.82	274.9	4.89×10^{-3}	15.73	284.5	5.75×10^{-3}	35.99	265.0	8.46×10^{-4}
7.82	274.7	4.94×10^{-3}	15.73	284.5	5.73×10^{-3}	35.99	265.0	8.37×10^{-4}
7.82	274.7	5.00×10^{-3}	15.73	279.6	4.03×10^{-3}	35.99	264.9	7.52×10^{-4}
7.82	269.9	3.40×10^{-3}	15.73	279.6	4.03×10^{-3}	35.99	264.8	8.04×10^{-4}
7.82	269.6	3.37×10^{-3}	15.73	279.5	4.18×10^{-3}	35.99	254.9	3.81×10^{-4}
7.82	265.0	2.34×10^{-3}	15.73	274.7	2.92×10^{-3}	35.99	254.6	3.40×10^{-4}
7.82	264.6	2.33×10^{-3}	15.73	274.7	2.80×10^{-3}	35.99	254.6	3.34×10^{-4}
7.82	260.1	1.40×10^{-3}	15.73	274.7	2.80×10^{-3}	35.99	244.7	1.08×10^{-4}
7.82	260.0	1.40×10^{-3}	15.73	269.7	1.91×10^{-3}	35.99	244.7	1.26×10^{-4}
7.82	259.9	1.61×10^{-3}	15.73	269.6	1.90×10^{-3}	35.99	244.6	1.11×10^{-4}
7.82	259.6	1.55×10^{-3}	15.73	269.5	1.97×10^{-3}	35.99	244.6	1.11×10^{-4}
7.82	255.3	9.22×10^{-4}	15.73	269.5	1.97×10^{-3}	35.99	239.7	7.33×10^{-5}
7.82	255.2	9.09×10^{-4}	15.73	264.8	1.26×10^{-3}	35.99	239.7	7.17×10^{-5}
7.82	255.1	9.12×10^{-4}	15.73	264.7	1.26×10^{-3}	35.99	234.8	3.96×10^{-5}
7.82	254.8	1.03×10^{-3}	15.73	264.4	1.33×10^{-3}	35.99	234.8	3.64×10^{-5}
7.82	254.8	1.02×10^{-3}	15.73	264.4	1.36×10^{-3}	35.99	234.8	3.82×10^{-5}
7.82	254.6	1.07×10^{-3}	15.73	264.4	1.34×10^{-3}	35.99	234.4	3.65×10^{-5}
7.82	250.2	6.00×10^{-4}	15.73	259.8	8.57×10^{-4}	35.99	230.3	2.65×10^{-5}
7.82	250.2	5.81×10^{-4}	15.73	259.8	8.61×10^{-4}	35.99	230.3	2.45×10^{-5}
7.82	250.2	5.98×10^{-4}	15.73	259.4	8.61×10^{-3}	35.99	225.8	1.28×10^{-5}
7.82	250.2	5.98×10^{-4}	15.73	254.7	5.27×10^{-4}	35.99	225.1	1.65×10^{-5}
7.82	250.2	6.00×10^{-4}	15.73	254.7	5.23×10^{-4}	35.99	225.0	1.13×10^{-5}
7.82	249.6	6.53×10^{-4}	15.73	254.7	5.29×10^{-4}	35.99	225.0	1.18×10^{-5}
7.82	249.6	6.75×10^{-4}	15.73	254.4	5.49×10^{-4}	35.99	225.0	1.24×10^{-5}
7.82	245.3	3.73×10^{-4}	15.73	254.4	5.57×10^{-4}	35.99	225.0	1.11×10^{-5}
7.82	245.2	3.75×10^{-4}	15.73	254.4	5.58×10^{-4}	35.99	225.0	1.16×10^{-5}
7.82	245.2	3.72×10^{-4}	15.73	249.6	3.41×10^{-4}	35.99	225.0	1.18×10^{-5}
7.82	245.1	3.67×10^{-4}	15.73	244.6	2.20×10^{-4}	35.99	224.9	1.31×10^{-5}
7.82	245.0	3.74×10^{-4}	15.73	239.7	1.40×10^{-4}	35.99	224.9	1.20×10^{-5}
7.82	244.8	4.18×10^{-4}	15.73	239.7	1.44×10^{-4}	35.99	224.9	1.48×10^{-5}
7.82	244.7	4.25×10^{-4}	15.73	239.7	1.39×10^{-4}	35.99	224.9	1.10×10^{-5}
7.82	244.7	4.41×10^{-4}	15.73	239.7	1.39×10^{-4}	35.99	224.8	1.08×10^{-5}
7.82	240.4	2.36×10^{-4}	15.73	239.7	1.40×10^{-4}	35.99	224.8	1.21×10^{-5}
7.82	239.8	2.75×10^{-4}	15.73	234.6	8.41×10^{-5}			
7.82	239.7	2.93×10^{-4}	15.73	234.6	6.99×10^{-5}			
7.82	235.6	1.39×10^{-4}	15.73	229.7	4.11×10^{-5}			
7.82	235.5	1.38×10^{-4}	15.73	224.7	2.59×10^{-5}			
7.82	234.9	1.76×10^{-4}	15.73	224.7	2.54×10^{-5}			
7.82	234.8	1.72×10^{-4}						
7.82	234.8	1.65×10^{-4}						
7.82	234.8	1.81×10^{-4}						
7.82	234.6	1.95×10^{-4}						
7.82	230.8	8.12×10^{-5}						
7.82	230.6	8.00×10^{-5}						
7.82	230.4	7.94×10^{-5}						
7.82	230.4	7.99×10^{-5}						
7.82	229.9	1.04×10^{-4}						
7.82	229.9	1.04×10^{-4}						
7.82	229.9	1.05×10^{-4}						
7.82	229.8	1.07×10^{-4}						
7.82	226.1	4.70×10^{-5}						
7.82	226.1	4.45×10^{-5}						
7.82	225.6	4.34×10^{-5}						
7.82	225.5	4.33×10^{-5}						
7.82	225.2	6.51×10^{-5}						
7.82	225.1	6.57×10^{-5}						
7.82	225.1	6.57×10^{-5}						
7.82	225.1	6.92×10^{-5}						
7.82	225.1	6.49×10^{-5}						
7.82	225.1	6.59×10^{-5}						

[a] Equilibrium total pressures above the 7.82 mol kg^{-1} solution were made on two separate occasions coinciding with a small modification of the cell lid. The resulting series of measurements, when combined, showed slightly more scatter at low temperatures than was observed in other experiments.

that $pHNO_3$ is more than 50% of the total pressure above the 35.99 mol kg^{-1} solution, but is less than 4% for the two more dilute solutions. Agreement with the model is satisfactory over the full temperature range (294.5_7 K to 224.6_5 K), though there

TABLE 2: Equilibrium Total Pressures (pH_2O + $pHCl$) above Aqueous HCl Solutions

*m*HCl (mol kg^{-1})	*T* (K)	*P* (atm)	*m*HCl (mol kg^{-1})	*T* (K)	*P* (atm)
9.45	279.7	4.88×10^{-3}	10.51	289.4	1.11×10^{-2}
9.45	279.7	4.86×10^{-3}	10.51	284.5	7.86×10^{-3}
9.45	274.9	3.38×10^{-3}	10.51	279.7	5.44×10^{-3}
9.45	274.9	3.38×10^{-3}	10.51	274.7	3.71×10^{-3}
9.45	274.8	3.38×10^{-3}	10.51	274.5	3.63×10^{-3}
9.45	274.8	3.40×10^{-3}	10.51	269.8	2.50×10^{-3}
9.45	274.8	3.36×10^{-3}	10.51	264.8	1.59×10^{-3}
9.45	274.7	3.36×10^{-3}	10.51	264.6	1.60×10^{-3}
9.45	274.6	3.31×10^{-3}	10.51	264.6	1.59×10^{-3}
9.45	272.1	2.72×10^{-3}	10.51	259.7	1.06×10^{-3}
9.45	272.0	2.72×10^{-3}	10.51	259.7	1.05×10^{-3}
9.45	264.8	1.52×10^{-3}	10.51	254.7	6.49×10^{-4}
9.45	264.8	1.51×10^{-3}	10.51	249.9	4.28×10^{-4}
9.45	264.7	1.51×10^{-3}	10.51	249.9	4.18×10^{-4}
9.45	264.7	1.51×10^{-3}	10.51	244.8	2.72×10^{-4}
9.45	264.7	1.51×10^{-3}	10.51	244.7	2.52×10^{-4}
9.45	264.7	1.51×10^{-3}	10.51	244.4	2.59×10^{-4}
9.45	261.3	1.13×10^{-3}	10.51	239.9	1.44×10^{-4}
9.45	261.2	1.12×10^{-3}	10.51	239.9	1.46×10^{-4}
9.45	256.7	7.61×10^{-4}	10.51	230.1	5.21×10^{-5}
9.45	256.0	7.15×10^{-4}	10.51	230.1	5.32×10^{-5}
9.45	255.0	6.51×10^{-4}	10.51	230.1	5.21×10^{-5}
9.45	254.9	6.51×10^{-4}	10.51	230.0	5.22×10^{-5}
9.45	254.9	6.52×10^{-4}	10.51	225.0	2.90×10^{-5}
9.45	254.9	6.49×10^{-4}	10.51	224.9	3.06×10^{-5}
9.45	250.7	4.45×10^{-4}	10.51	224.9	3.01×10^{-5}
9.45	244.9	2.66×10^{-4}	10.51	219.7	1.65×10^{-5}
9.45	244.9	2.65×10^{-4}	10.51	215.0	8.50×10^{-6}
9.45	244.9	2.66×10^{-4}	10.51	214.9	1.02×10^{-5}
9.45	244.9	2.66×10^{-4}	10.51	214.9	9.23×10^{-6}
9.45	244.9	2.65×10^{-4}	10.51	209.8	4.84×10^{-6}
9.45	244.9	2.67×10^{-4}	10.51	205.0	2.44×10^{-6}
9.45	241.3	1.88×10^{-4}			
9.45	241.2	1.87×10^{-4}			
9.45	240.3	1.71×10^{-4}			
9.45	235.2	9.20×10^{-5}			
9.45	234.6	8.65×10^{-5}			
9.45	234.6	8.83×10^{-5}			
9.45	234.6	8.57×10^{-5}			
9.45	234.6	8.60×10^{-5}			
9.45	230.9	5.67×10^{-5}			
9.45	229.6	4.92×10^{-5}			
9.45	225.4	3.03×10^{-5}			
9.45	224.6	2.74×10^{-5}			
9.45	224.6	2.93×10^{-5}			
9.45	224.6	2.82×10^{-5}			
9.45	221.0	1.79×10^{-5}			
9.45	219.7	1.59×10^{-5}			
9.45	215.6	9.72×10^{-6}			
9.45	214.9	8.90×10^{-6}			
9.45	214.9	8.58×10^{-6}			
9.45	211.2	5.64×10^{-6}			
9.45	210.0	4.52×10^{-6}			
9.45	204.6	2.54×10^{-6}			
9.45	204.6	2.44×10^{-6}			
9.45	204.6	2.30×10^{-6}			
9.45	199.5	1.26×10^{-6}			

is a large scatter in the data for the 7.82 mol kg^{-1} solution for which the measurements were carried out in two stages (see notes to Table 1). Deviations are plotted in Figure 3b. A small positive offset is apparent for the 7.82 and 15.73 mol kg^{-1} solutions at high temperatures, and scatter increases at low temperatures, but overall there is no apparent trend.

Measured pHNO$_3$ over 15.73 mol kg^{-1} HNO_3 (Table 3) are compared with calculated values in Figure 4. The model appears to predict the partial pressures well, though data are scattered by about +10% to −50% (see inset to Figure 4).

The model of Carslaw et al.[2] is based, for HNO_3−H_2O solutions, on the earlier work of Clegg and Brimblecombe.[3] These authors included the low temperature partial pressure

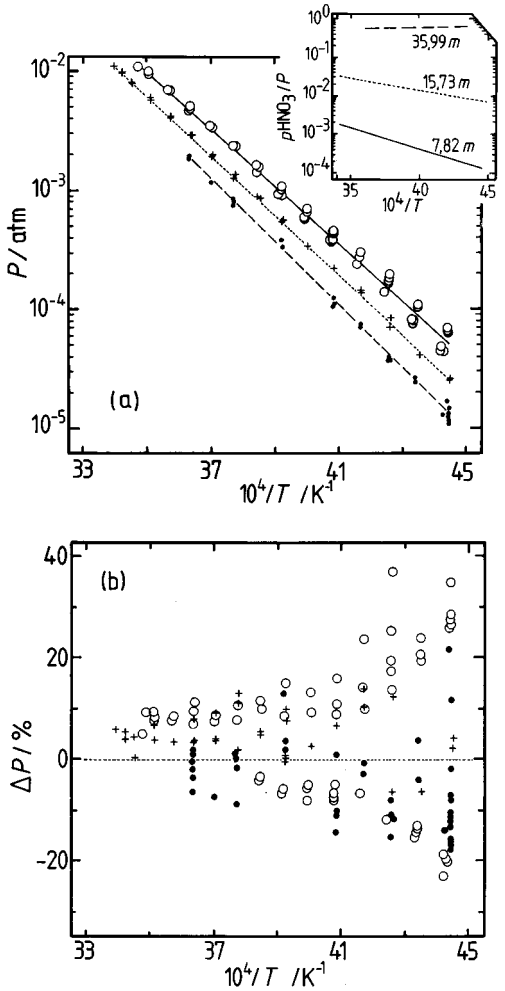

Figure 3. Equilibrium total pressures (P) above aqueous HNO_3 solutions to low temperature. Data are from Table 1. (a) Symbols: (open circle) 7.82 mol kg^{-1}, (plus) 15.73 mol kg^{-1}, (dot) 35.99 mol kg^{-1}. Lines: predictions of the model of Carslaw et al.[2] The inset shows the calculated fraction of the total pressure due to $HNO_{3(g)}$ for the three test solutions. (b) Percentage deviations, calculated as $100(P_{meas} - P_{calc})/P_{calc}$. Symbols as in (a) above.

TABLE 3: Equilibrium Partial Pressures of HCl and HNO_3 above Their Pure Aqueous Solutions

*m*HCl (mol kg^{-1})	*T* (K)	pHCl (atm)	*m*HNO$_3$ (mol kg^{-1})	*T* (K)	pHNO$_3$ (atm)
9.45	274.8	4.23×10^{-4}	15.73	265.0	2.41×10^{-5}
9.45	264.7	2.38×10^{-4}	15.73	264.6	2.27×10^{-5}
9.45	254.9	9.32×10^{-5}	15.73	255.2	6.99×10^{-6}
9.45	244.9	2.80×10^{-5}	15.73	255.0	5.00×10^{-6}
9.45	234.6	1.29×10^{-5}	15.73	250.7	4.21×10^{-6}
10.51	284.1	3.24×10^{-3}	15.73	250.5	4.63×10^{-6}
10.51	274.5	1.32×10^{-3}	15.73	250.4	5.32×10^{-6}
10.51	264.5	4.38×10^{-4}	15.73	240.1	1.71×10^{-6}
10.51	259.4	3.88×10^{-4}			
10.51	254.6	1.04×10^{-4}			
10.51	249.4	1.11×10^{-4}			
10.51	244.8	1.32×10^{-4}			
10.51	239.4	4.61×10^{-5}			

measurements of Hanson and Mauersberger[9] in their correlation. The present results, in broadly confirming the model for the concentrations and temperatures studied, are therefore also consistent with the earlier data.

4.2. HCl−H_2O. Total pressures above 9.45 and 10.51 mol kg^{-1} HCl determined in this study are compared with predictions of the model of Carslaw et al. in Figure 5. These relatively

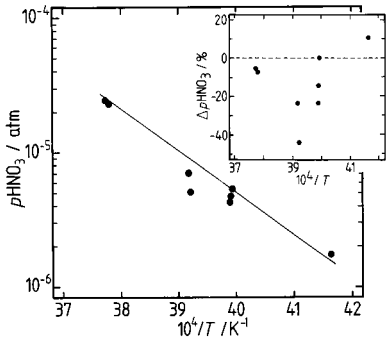

Figure 4. Equilibrium partial pressures of HNO_3 ($pHNO_3$) above 15.73 mol kg^{-1} aqueous HNO_3. Symbols: measurements from this study (Table 3). Line: predictions of the model of Carslaw et al.[2] Inset: deviations from the model.

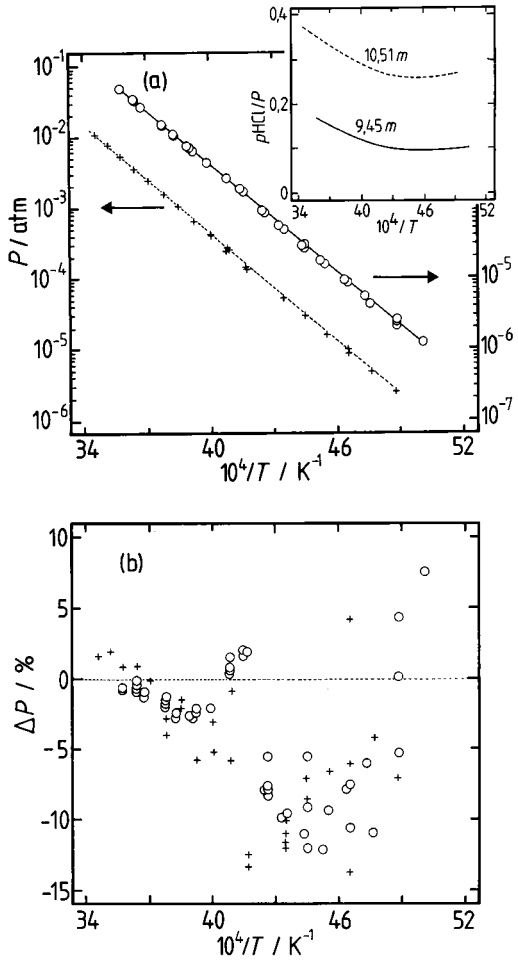

Figure 5. Equilibrium total pressures (P) above aqueous HCl solutions to low temperature. Data are from Table 2. (a) Symbols: (open circle) 9.45 mol kg^{-1}, (plus) 10.51 mol kg^{-1}. Lines: predictions of the model of Carslaw et al.[2] Note the use of two pressure scales. The inset shows the calculated fraction of the total pressure due to $HCl_{(g)}$ for the two test solutions. (b) Percentage deviations, calculated as $100(P_{meas} - P_{calc})/P_{calc}$. Symbols as in (a) above.

concentrated solutions were chosen, first, to generate partial pressures of HCl that would make a significant contribution to the total pressure and, second, to be representative of solutions with the strong H^+-Cl^- interactions that would be expected in highly acidic stratospheric aerosols. Figure 5a shows that there is reasonable agreement to 200 K with the model of Carslaw et al.,[2] which we note is based chiefly upon data for temperatures ≥273.15 K (see section IV of Carslaw et al.[2]). The calculated

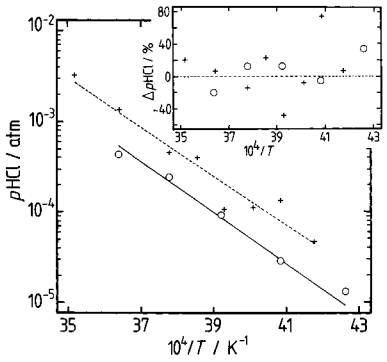

Figure 6. Equilibrium partial pressures of HCl (pHCl) above aqueous HCl solutions to low temperature. Data are from Table 3. Symbols: (open circle) 9.45 mol kg^{-1}, (plus) 10.51 mol kg^{-1}. Lines: predictions of the model of Carslaw et al.[2] The inset shows the percentage deviations, calculated as $100(p\mathrm{HCl}_{meas} - p\mathrm{HCl}_{calc})/p\mathrm{HCl}_{calc}$. Symbols as in the main plot.

partial pressure fraction of HCl ranges from about 0.09 to 0.38 for the two solutions. Deviations in the total pressure are plotted in Figure 5b, which shows a small negative trend with decreasing temperature for both solutions, the measured pressures being about 10% lower than the calculated values at ~220 K. The experimentally determined partial pressures of HCl over the two solutions are compared with model predictions in Figure 6. No clear trend is seen in the deviations, although it is possible that the calculated pHCl are up to 40% too low at the lowest temperatures. In terms of aqueous activities this implies that the calculated activity coefficient product $f_H{}^* f^*_{Cl}$ is too low, with an opposite (though probably smaller) error in the water activity. As water is calculated to contribute about 90% to the total pressure above the 9.45 mol kg^{-1} solution, such an error might account for at least some of the observed differences between calculated and measured total pressure.

Tests were carried out to determine whether differences between the activity coefficient model parameterization of Carslaw et al.[2] and the data to which the model was fitted could account for the deviations shown in Figure 5. However, pHCl calculated using activity coefficients directly from the model of Carslaw et al. differed by <2% from values determined using measured activity coefficients at 298.15 K together with partial molar enthalpies and heat capacities. Differences in the water activity (hence pH_2O) were also very small.

The only other measurements of pH_2O and pHCl at low temperature are those of Miller,[10] for HCl mole fractions of 0.0411 (2.379 mol kg^{-1}) to 0.2145 (15.16 mol kg^{-1}). Miller obtained 1.237×10^{-4} atm total pressure and a pHCl fraction of 0.12 for a mole fraction of 0.1545 (10.14 mol kg^{-1}) at 238.15 K, compared to 1.351×10^{-4} atm (pHCl fraction equal to 0.20) predicted by the model. The deviation in total pressure is −8.5%, and is consistent with that shown by our own measurements in Figure 5b. However, the pHCl determined by Miller[10] above 10.14 mol kg^{-1} HCl at 238.15 K is 1.451×10^{-5} atm compared with a predicted value of 2.694×10^{-5} atm, close to a factor of 2 different. The pHCl determined in this study for 9.45 mol kg^{-1} and 10.51 mol kg^{-1} solutions agree with the model predictions more closely than does the value of Miller[10] at this temperature.

It is concluded that, at least for the molalities of about 10 mol kg^{-1} studied here, the model of Carslaw et al.[2] may predict total pressures up to about 10% too high at low temperature. If so, then most of this is likely to be due to positive errors in the predicted water partial pressure, implying that the calculated

*p*HCl (which constitutes a relatively small fraction of the total equilibrium pressure) may be too low. However, the fact that the trend in the deviations between measured and calculated pressures (Figure 5b) begins at about 273.15 K is surprising, as the activity coefficients of aqueous HCl are well defined over a large range of temperatures from 273.15 K to >323.15 K.

4.3. HCl−HNO_3−H_2O. The model of Carslaw et al.[2] is not parameterized for $H^+-Cl^--NO_3^-$ interactions, due to a lack of data. Measurements of total and partial pressures above an acid mixture containing 15.7 mol kg^{-1} HNO_3 and 2.15 mol kg^{-1} HCl were therefore attempted. However, after the test solution had been degassed to remove dissolved air, a continuously rising total pressure was observed (to more than 10 times the expected value), with small bubbles of gas being generated in the solution.

The reaction in the test cell is believed to be that occurring in aqua regia, a mixture of concentrated HNO_3 and HCl usually prepared as one part HNO_3 and two to four parts HCl:[5]

$$3HCl + HNO_3 \rightleftharpoons NOCl + Cl_2 + 2H_2O \qquad (9)$$

In a closed system the reaction is reversible,[5] with an equilibrium pressure of 2.84 atm at 273.15 K. The equilibrium pressure of the system diminishes with dilution with water. The reaction has been studied conductimetrically in dilute solutions by Oishi,[11] at a concentration of about N/10. This author obtained results consistent with the above reaction, combined with hydrolysis of NOCl:

$$NOCl_{(aq)} + H_2O_{(l)} \rightleftharpoons HNO_{2(aq)} + HCl_{(aq)} \qquad (10)$$

yielding a net overall reaction $2HCl_{(aq)} + HNO_{3(aq)} \rightleftharpoons HNO_{2(aq)} + Cl_{2(aq)} + H_2O_{(l)}$. In the more concentrated solutions studied here, reaction 10 would not be expected to go to completion, thus both NOCl and HNO_2 might exist as products. We have estimated the equilibrium compositions of the HNO_3−HCl−H_2O test solutions, and the partial pressures of the volatile species, as follows. First, reactions 9 and 10 are rewritten on the basis of stoichiometric dissociation of the strong acids HNO_3 and HCl in order to use the model of Carslaw et al.[2] to calculate ion activities:

$$4H^+_{(aq)} + NO_3^-{}_{(aq)} + 3Cl^-_{(aq)} \rightleftharpoons NOCl_{(aq)} + Cl_{2(aq)} + 2H_2O_{(l)} \qquad (11)$$

$$NOCl_{(aq)} + H_2O_{(l)} \rightleftharpoons HNO_{2(aq)} + H^+_{(aq)} + Cl^-_{(aq)} \qquad (12)$$

The weak acid HNO_2 will exist only as the neutral molecule in the test solutions, though it could undergo the further reaction:

$$2HNO_{2(aq)} \rightleftharpoons NO_{(aq)} + NO_{2(aq)} + H_2O_{(l)} \qquad (13)$$

Gibbs energies and heats of formation at 298.15 K for all species were taken from available sources of data (see Appendix IV), and used to calculate equilibrium constants for reactions 11 to 13 and Henry's law constants for the gases Cl_2, NOCl, HNO_2, NO, and NO_2. The water activity in the test solutions, and activities of the ions H^+, NO_3^-, and Cl^- were calculated using the model of Carslaw et al.[2] All other species were assigned unit activity coefficients. The three equilibrium equations for reactions 11 to 13 above were then solved for the molalities of the aqueous species. The results are shown in Figure 7.

Over the measured temperature range of 205.4−264.8 K, $Cl_{2(g)}$ is predicted to make up more than 90% of the calculated total pressure above the solution, NOCl about 2−7%, and all other gases <0.4%. The calculated pCl_2 at 264.8 K is 0.27 atm for an equilibrium molality of 0.054 mol kg^{-1}.

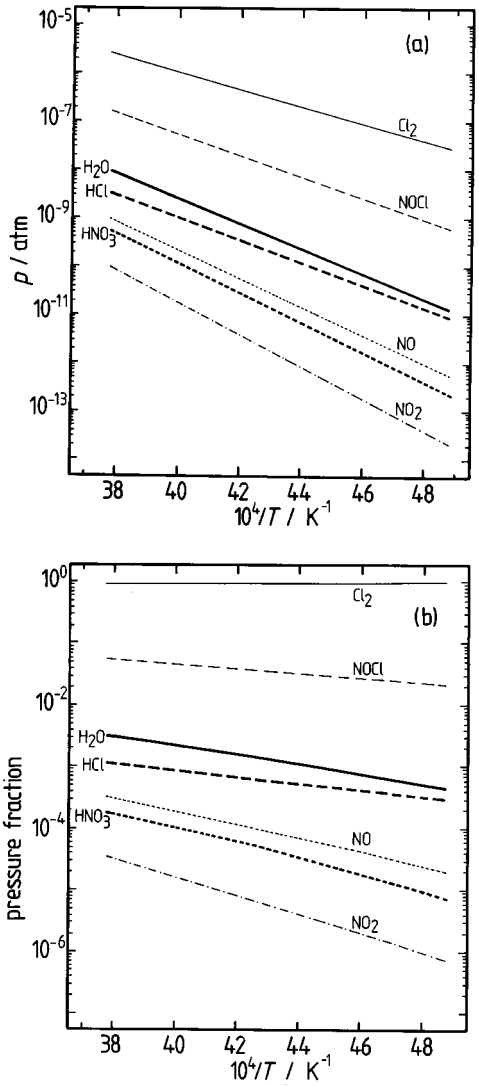

Figure 7. Calculated equilibrium partial pressures of gases above a solution containing 15.7 mol kg^{-1} HNO_3 and 2.15 mol kg^{-1} HCl, taking into account the reactions given in eq 11 to eq 13. (a) Partial pressures of each gas. (b) The fractional contribution of each gas to the calculated total pressure above the solution.

An equilibrium total pressure of 5.72×10^{-3} atm was determined at 205.4 K. This was the only stable pressure observed. The predicted pressure from reactions 11−13 is 3.45×10^{-3} atm, which agrees well with the measured value considering the lack of thermodynamic data needed to calculate accurately equilibria in the test solution at very low temperature. Almost all of the pressure (98%) is calculated to be due to Cl_2, with the total partial pressures of H_2O, HNO_3 and HCl amounting to only 2.5×10^{-6} atm.

Some partial pressures of Cl-containing gases and N-containing gases were determined for non-equilibrium conditions in the test cell (during degassing). As described in section 3.3 these measurements are based upon counts of the fragments $m/z = 30$ (NO^+) and $m/z = 35$ (Cl^+), and the assumption that the gases were NOCl and Cl_2. The ratio pCl_2/pNOCl was found to decrease with increasing temperature, from about 2−3 at 205 K to <0.7 at 264 K. In contrast, the calculated equilibrium partial pressure of NOCl is less than that of Cl_2 by more than

a factor of 10 at all temperatures (Figure 7), though the predicted trend in the ratio is similar to that observed: from about 48 at 205 K to 16 at 264 K (a decrease of a factor of 3).

How rapid is the reaction in the $HCl-HNO_3-H_2O$ solution? While no direct measurements were made, it was noted that the increase in total pressure in the test cell following degassing (to remove dissolved air) occurred slowly: typically at a rate of about 5×10^{-6} atm min^{-1}. By contrast, the rise in total pressure to the equilibrium values for the pure aqueous HCl and HNO_3 solutions was close to instantaneous. This suggests that the time scale of reactions 11 to 13, including the transfer of Cl_2 and NOCl to the gas phase is of the order of minutes to hours. If so, this might explain why Cl_2 generation was not observed in experiments involving solutions containing both HCl and HNO_3 and carried out using flow tubes.[12,13]

5. Discussion

Reactions 11 and 12 have been shown to produce significant partial pressures of Cl_2, or Cl-containing gases, above the $HNO_3-HCl-H_2O$ solutions studied here. Could the reaction be important in liquid stratospheric aerosols, where dissolved HNO_3 and HCl are present at much lower concentrations? An important factor in the atmosphere is the rates of the reactions compared to others that consume HCl within or on the surface of aerosols. Our experiments give no quantitative information on the kinetics of the reaction. However, it is worth estimating the equilibrium composition of the aerosol with respect to Cl_2 and other volatile reaction products in order to determine whether it could potentially contribute to the production of active chlorine. We have done this for an atmosphere containing 0.5 ppbv H_2SO_4, 5 ppmv H_2O, 10 ppbv HNO_3, and 2 ppbv HCl at 50 mb pressure over the temperature range 210−185 K. This composition corresponds closely to a case in the northern polar stratosphere observed by Dye et al.[14] and previously modeled by Carslaw et al.[15] Figure 8 shows calculated molalities of H_2SO_4, HNO_3, and HCl in the supercooled liquid aerosol droplets. Note that all H_2SO_4 resides in the aerosol phase, and its decreasing molality is due to the simultaneous uptake of water and HNO_3 as temperature falls. The concentration of HCl in the aerosol increases with falling temperature, partly due to the increase in its Henry's law constant but mostly due to the decrease in acidity caused by dilution by the condensing water vapor. Figure 9 shows calculated equilibrium partial pressures and mixing ratios of Cl_2, NOCl, NO and NO_2 for the aerosol compositions and temperatures in Figure 8, and assuming reactions 11−13 to occur. Above 190 K the equilibrium pCl_2 varies relatively little, even though the HCl concentration falls. This is because the activity of the H^+ ion in the aqueous aerosol rises steeply with temperature, and reaction 11 depends on the activity of H^+ raised to the power 4. The calculated equilibrium partial pressure of Cl_2 ranges from about $2-5 \times 10^{-9}$ atm. This would correspond to a mixing ratio of up to about 80 ppbv at 50 mb.

On equilibrium grounds, and neglecting kinetics, it appears possible that reactions 11 and 12 could produce significant amounts of Cl_2 even if our calculations are in error by an order of magnitude. Furthermore, this could apply even at temperatures above 210 K due to the relatively low sensitivity of calculated pCl_2 to temperature. It is important, therefore, to investigate the rates of reactions 11 and 12 for aqueous solutions at very low temperature and for the compositions expected in aqueous stratospheric aerosols.

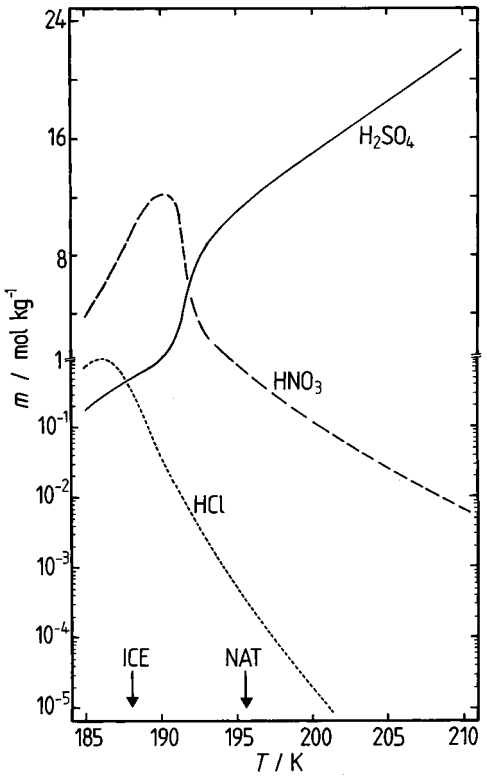

Figure 8. Calculated composition of an aqueous aerosol at 50 mb altitude, in an airmass containing 0.5 ppbv H_2SO_4, 5 ppmv H_2O, 10 ppbv HNO_3, and 2 ppbv HCl. The temperatures at which the liquid aerosol becomes saturated with respect to NAT and ice are marked by vertical arrows.

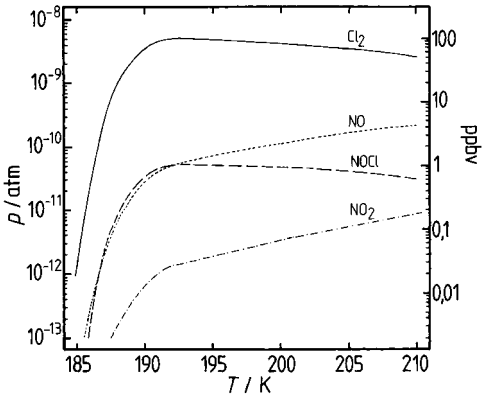

Figure 9. Calculated equilibrium partial pressures (p) of trace gases, and equivalent mixing ratios at 50 mb altitude (in ppbv), for the aqueous aerosol compositions and temperatures shown in Figure 8.

6. Summary and Conclusion

In this work we have measured equilibrium total and partial pressures above aqueous HCl and HNO_3 solutions to low temperature. The results of the experiments for aqueous HNO_3 are consistent with predictions of the model of Carslaw et al.,[2] within experimental uncertainty.

In Appendix I the correlation of Clegg and Brimblecombe[3] of HNO_3 and H_2O activities in aqueous HNO_3 has been revised to take into account recent measurements of the heat capacities of the solutions. However, this results in differences in predicted partial pressures of HNO_3 and H_2O of less than about 10%, even at stratospheric temperatures. These are smaller than the errors introduced by the parameterization of the results into the model of Carslaw et al.,[2] which is necessary in order to enable calculations for multicomponent solutions to be carried out.

In Appendix II the vapor pressure products (K_P) of the three (solid) nitric acid hydrates have been evaluated from literature data, and best fit equations are presented. These equations are based upon the values of K_P and the enthalpy change for the reaction at the melting point of the solid, and the known heat capacity difference between the solid and gas-phase water and HNO_3 as a function of temperature. The aqueous activity product (^xK_S) of nitric acid dihydrate has also been determined, and included in the model of Carslaw et al.[2] The model has been shown to predict partial pressures and effective Henry's law constants (H^*) of HCl and HNO_3 that agree satisfactorily with the few available data for multicomponent acid solutions.

Literature data for HBr solubilities in aqueous H_2SO_4, and equilibrium partial pressures of HBr above $HBr-H_2SO_4-H_2O$ solutions, have been used to improve the model of Carslaw et al.[2] for this system (Appendix III). The changes involve a revision to the equation for the Henry's law constant of HBr and the introduction into the activity coefficient equations of parameters to account for interactions between H^+, HSO_4^-, SO_4^{2-}, and Br^- ions. The revised model agrees well with experimental data from several sources and should yield improved predictions of HBr solubility in stratospheric aerosols.

Total and partial pressures of water and HCl above aqueous HCl measured in this study agree satisfactorily with model predictions, though there is a systematic deviation between measured and calculated total pressure of about 10% at 220 K. This appears to be consistent with the results of the only other study that has been carried out at low temperature.[10] Calculated equilibrium partial pressures above $HCl-HNO_3-H_2SO_4-H_2O$ solutions at stratospheric temperatures also agree with the available literature data (Appendix III), though the number of measurements are few. Our own experiments to determine total and partial pressures above an $HCl-HNO_3-H_2O$ solution showed that HCl and HNO_3 reacted, yielding a total pressure orders of magnitude greater than predicted for H_2O, HNO_3 and HCl alone. Mass spectrometric measurements showed that the vapor phase contained mostly Cl-containing gases, almost certainly Cl_2. Equilibrium thermodynamic calculations support this, and show that reactions yielding Cl_2 and NOCl, known to occur in aqua regia, could account for the experimental observations. Further calculations for aqueous solutions of stratospheric aerosol composition suggest, solely on an equilibrium basis, that the reaction might be a source of active chlorine in the atmosphere. However, the experiments imply that the reactions are slow.

Appendix I

Osmotic and Activity Coefficients of Aqueous HNO_3. The model of Carslaw et al.[2] for this system is based upon the earlier study of Clegg and Brimblecombe.[3] These authors used measurements of equilibrium pH_2O and $pHNO_3$, and thermal and solubility data to derive equations for solute and solvent activities and partial pressures over the entire composition range as a function of temperature. Equilibrium constants (^xK_S) for the solids $HNO_3 \cdot 3H_2O_{(cr)}$ and $HNO_3 \cdot H_2O_{(cr)}$ were derived from solubility and partial pressure product data. Clegg and Brimblecombe[3] noted the publication by Hovey et al.[16] of heat capacities of 0.1116 to 1.1115 mol kg^{-1} HNO_3 over the temperature range 283.15−328.15 K, though these data were not used in their work. Here, the correlation of Clegg and Brimblecombe[3] is revised for the Henry's law constant of HNO_3 and differentials of the partial molar enthalpies (J_1 and J_2) with respect to temperature. The data of Hovey et al.[16] were first used to determine values of $\partial^\phi C_p/\partial T$ from 0.1116 to 1.1115 mol kg^{-1}. These differentials were then combined with values for concentrated solutions obtained from the results of Mishchenko[17] to produce the following expression for $\partial^\phi C_p/\partial T$ at 298.15 K, valid over the entire composition range:

$$\partial^\phi C_p/\partial T = 1.622 + 1.004377 I_x^{1/2} - 12.2274 I_x^{3/4} + 9.830074 I_x \quad \text{(A1)}$$

where $^\phi C_p$ (J $mol\ K^{-1}$) is the apparent molar heat capacity, and I_x is the mole fraction ionic strength of the solution, equivalent to $m HNO_3/(2m HNO_3 + 55.508681)$. This expression replaces eq 28 of Clegg and Brimblecombe[3] and is used to calculate the following equations for the differentials with respect to temperature of the partial molar heat capacities of water (Γ_1) and HNO_3 (Γ_2) in solution:

$$\Gamma_1 = -I_x^2(9.830074 + 0.5021885 I_x^{-1/2} - 9.17055 I_x^{-1/4}) \quad \text{(A2)}$$

$$\Gamma_2 = 19.660148 I_x(1 - I_x) + 1.004377 I_x^{1/2}(1.5 - I_x) - 12.2274 I_x^{3/4}(1.75 - 1.5 I_x) \quad \text{(A3)}$$

The infinite dilution value of $\partial^\phi C_p/\partial T$ implied by eq A1 (1.622 J mol^{-1} K^{-2}) then replaces the second and third terms in eq 36 of Clegg and Brimblecombe[3] (for the variation of $^\phi C_p^\circ$ with temperature), yielding a new expression for the Henry's law constant ^xK_H:

$$^xK_H = 6.74888 - 72.3 \times 10^3(1/T_r - 1/T)/R - 577.8992(T_r/T - 1 + \ln(T/T_r))/R + 1.508666(T_r(T_r/T - 1) + T - T_r)/2R + 0.0310414 \times 10^{-3}(2T_r^2(T_r/T - 1) + T^2 - T_r^2)/6R \quad \text{(A4)}$$

The revised equations for activities are compared, in terms of calculated equilibrium $pHNO_3$, with the original work of Clegg and Brimblecombe[3] in Figure 10a. The predicted partial pressures differ by up to 10% at the lowest temperatures, with the revised correlation giving lower values. The model of Carslaw et al.,[2] in which aqueous activities are calculated using the Pitzer−Simonson−Clegg model[6] fitted to activities calculated from the work of Clegg and Brimblecombe,[3] is compared with the revised correlation in Figure 10b. Differences remain below +10% to −15% for concentrations below 70 mass %. The increase at higher concentrations is due to the restricted fit by Carslaw et al.[2] to ≤72 mass% for $T < 219$ K and ≤85 mass % at higher temperatures. Calculated water partial pressures agree more closely: the original correlation of Clegg and Brimblecombe[3] and its revision differ by <1% where the same expression for the vapor pressure of pure water[4] is used. Figure 11 compares water partial pressures calculated from the revised correlation with those from the model of Carslaw et al.[2] Differences only exceed 1% for concentrations of >50 mass %, where accuracy is limited by the fit of the Pitzer−Simonson−Clegg activity model.

Equilibrium partial pressures of HNO_3 and H_2O above supercooled aqueous HNO_3 have not been measured to low enough temperature, or with sufficient precision, to determine whether the revised activity correlation is more accurate. However, it is clear that, first, differences remain small at all but the lowest stratospheric temperatures. Second, the differences are less than the inaccuracies introduced by the parameterization of the results into the model of Carslaw et al.[2] which is used to estimate the properties of mixtures. At present a

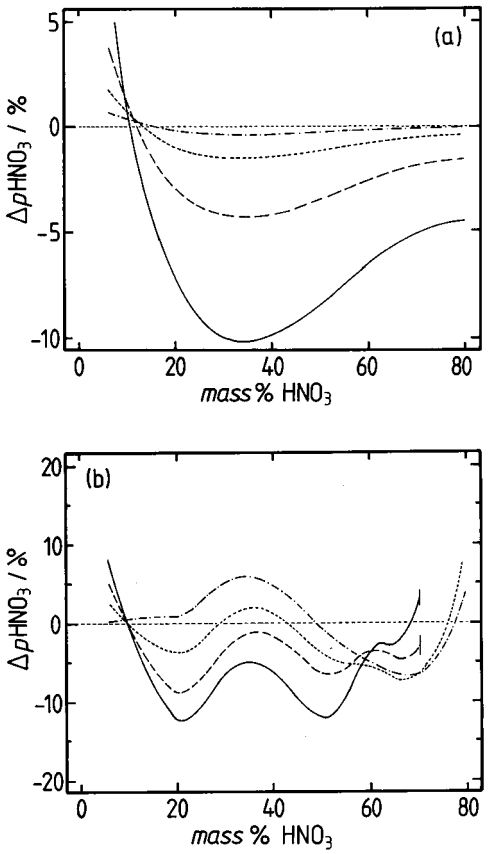

Figure 10. (a) Difference between equilibrium HNO_3 partial pressures above aqueous HNO_3 calculated using the revised correlation of Clegg and Brimblecombe (see Appendix I), and their original work.[3] ($\Delta pHNO_3$ is positive where the revised correlation yields a higher partial pressure.) Lines: (solid) 190 K, (dashed) 210 K; (dotted) 230 K, (dash/dot) 250 K. (b) Difference between equilibrium HNO_3 partial pressures above aqueous HNO_3 calculated using the revised correlation of Clegg and Brimblecombe (see Appendix I), and the model of Carslaw et al.[2] ($\Delta pHNO_3$ is positive where the revised correlation yields a higher partial pressure.) Lines: temperatures as in (a) above. The truncation of the lines at the two lowest temperatures in corresponds to the maximum molality to which the model of Carslaw et al.[2] was fitted.

change to the parameterization of the model for HNO_3-H_2O interactions is therefore not needed. We have, however, used the revised activity correlation and Henry's law constant expression in the evaluations of K_P for HNO_3 hydrates presented below.

Appendix II

Vapor Pressures of the Solid HNO_3 Hydrates. Values of K_P for the HNO_3 hydrates can be calculated from the aqueous activities of solutions in equilibrium with the solid, and should agree with partial pressure products $pHNO_3 \cdot pH_2O^n$ determined directly over the solids at the same temperature. In the evaluations of available K_P data presented below, partial pressures of HNO_3 and H_2O above the saturated solutions are calculated using the revision of the correlation of Clegg and Brimblecombe[3] together with the corresponding Henry's law constant (see Appendix I). Sources of solid/vapor equilibrium data for HNO_3 hydrates are listed in Table 4.

First we consider nitric acid trihydrate (NAT), the most extensively studied and atmospherically important of the hydrates. Figure 12 shows $\ln(K_P[\mathrm{NAT}])$ for $190 \le T \le 255.71$ K, distinguishing those values (in the upper left of the plot)

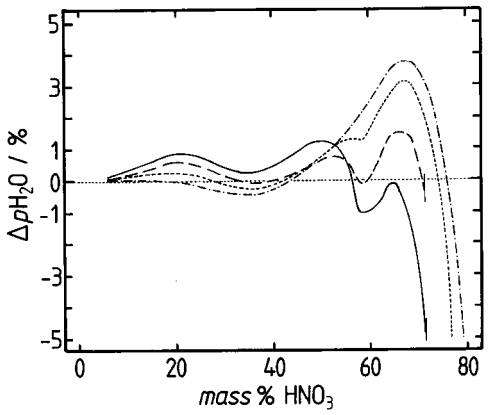

Figure 11. Difference between equilibrium water partial pressures above aqueous HNO_3 calculated using the revised correlation of Clegg and Brimblecombe (see Appendix I), and the model of Carslaw et al.[2] (ΔpH_2O is positive where the revised correlation yields a higher partial pressure). Lines: (solid) 190 K, (dashed) 210 K; (dotted) 230 K, (dash/dot) 250 K. The truncation of the lines at the two lowest temperatures corresponds to the maximum molality to which the model of Carslaw et al.[2] was fitted.

obtained from the aqueous solubilities of Kuster and Kremen,[18] and Pickering,[19] together with the revised correlation of activities in aqueous HNO_3 presented in Appendix I. There is satisfactory consistency overall. Heat capacities of the solid have been measured by Forsythe and Giauque[20] as a function of temperature, and those of $HNO_{3(g)}$ and $H_2O_{(g)}$ are also available.[21] These heat capacities have been fitted as functions of temperature, and used to calculate the $\Delta_r C_p$ element of the expression for K_P(NAT) (terms Δa to Δe in eq 8). Forsythe and Giauque[20] have also determined a melting temperature of 254.63 K for NAT. At this temperature, and for a molality of 18.503 mol kg^{-1} (1:3 HNO_3:H_2O), we calculate K_P(NAT) equal to 1.2429×10^{-15} atm^4. Using 254.63 K as a reference temperature we can now compare all data in terms of $\Delta_r H°$, the enthalpy change for the reaction at the melting temperature. Values of $\Delta_r H°$ are calculated as:

$$\begin{aligned}\Delta_r H° = (R\ln(K_{P(T)}) - R\ln(K_{P(T_r)}) - \\ \Delta a(T_r/T - 1 + \ln(T/T_r)) - \\ \Delta b(T_r(T_r/T - 1) + T - T_r)/2 - \\ \Delta c(2T_r^2(T_r/T - 1) + T^2 - T_r^2)/6 - \\ \Delta d(3T_r^3(T_r/T - 1) + T^3 - T_r^3)/12 - \\ \Delta e(1.5T_r^{1.5}(T_r/T - 1) + \\ T^{1.5} - T_r^{1.5})/3.75)/(1/T_r - 1/T) \quad \text{(A5)}\end{aligned}$$

where $\ln(K_{P(T)})$ is the experimental value of the partial pressure product at temperature T, and $\ln(K_{P(T_r)})$ (−34.321) is the reference value at the melting temperature T_r. This approach, using the melting temperature as reference for the equilibrium constant and enthalpy change, is the same as that used in the earlier study of Wooldridge et al.[40] The value of $\Delta_r H°$ obtained from eq A5 should be a constant, though errors can be expected to increase at higher temperatures where the difference between the experimental $\ln(K_{P(T)})$ and $\ln(K_{P(T_r)})$ becomes small relative to the precision of the measurement. Calculated values of $\Delta_r H°$ derived from all data sources are plotted in Figure 13, together with contours showing the effect of 1−10 % errors in the experimental K_P. There is generally good agreement, with no overall trend with temperature, though K_P calculated from

TABLE 4: Sources of Thermodynamic Data for Solid−Vapor Equilibrium of HNO_3 Hydrates[a]

hydrate[b]	used[c]	data type[d]	T (K)	source
NAT	yes	$pHNO_3$, pH_2O[e]	190−205	Hanson and Mauersberger[23]
NAT	no	$pHNO_3$, pH_2O	191−197	Hanson and Ravishankara[26]
NAT	no	$pHNO_3 \times pH_2O^3$	190−230	Worsnop et al.[22]
NAT, αNAT	no	$pHNO_3 \times pH_2O^3$	189−210	Fox et al.[25]
NAT/solution	no	$pHNO_3$, pH_2O	256−233	Hanson and Mauersberger[9]
NAT/ice	no	$pHNO_3$, pH_2O	190−230	Hanson and Mauersberger[9]
NAT/ice	yes	$pHNO_3$, pH_2O[e]	190−230	Hanson and Mauersberger[23]
NAT/NAM	yes	$pHNO_3$, pH_2O[f]	190−230	Hanson and Mauersberger[9]
NAT/NAM	yes	$pHNO_3$, pH_2O[e,f]	190−230	Hanson and Mauersberger[23]
NAD	no	$pHNO_3 \times pH_2O^2$	190−215	Worsnop et al.[22]
NAD	yes	$pHNO_3 \times pH_2O^2$[g]	189−198	Fox et al.[25]
NAD	yes	$pHNO_3$, pH_2O[g]	191	Hanson and Ravishankara[26]
NAM	yes	$pHNO_3 \times pH_2O$[f]	190−216	Worsnop et al.[22]

[a] Most of the results referenced above were presented graphically and in terms of fitted equations. Data were extracted from the graphs in a few cases, otherwise the equations were used over the temperature ranges of the original measurements. [b] NAT−$HNO_3 \cdot 3H_2O_{(cr)}$, NAD−$HNO_3 \cdot 2H_2O_{(cr)}$, NAM−$HNO_3 \cdot H_2O_{(cr)}$. [c] Used in the fit of the equilibrium constants. [d] Individual HNO_3 and H_2O partial pressures, or partial pressure product. [e] Fit of the NAT equilibrium constant (K_P) uses these data, together with freezing points[18,32] (with respect to NAT) and activity coefficients and ${}^xK_H(HNO_3)$ from this study. [f] Fit of the NAM equilibrium constant (K_P) uses these data, together with freezing points[18,32] (with respect to NAM) and activity coefficients and ${}^xK_H(HNO_3)$ presented in this work. [g] Fit of the NAD equilibrium constant (K_P) uses these data, together with freezing points (with respect to NAD) of Ji and Petit[24] and activity coefficients and ${}^xK_H(HNO_3)$ presented in this work.

the fitting equations of Worsnop et al.,[22] and Hanson and Mauersberger[9] for the trihydrate/monohydrate boundary, are discordant to a small degree with other data. Some values of K_P obtained by Hanson and Mauersberger[9] over solutions in equilibrium with solid NAT yield $\Delta_r H°$ that appear to be low. Upon the basis of the comparison in Figure 13, we have fitted the data of Hanson and Mauersberger[23] and K_P calculated from $HNO_3 \cdot 3H_2O_{(cr)}$ solubilities to obtain $\Delta_r H° = 229.66 \pm 0.14$ kJ mol^{-1} at 254.63 K and the following expression for the equilibrium constant:

$$\ln(K_P[\mathrm{NAT}]) = -34.321 + 229.66 \times 10^3(1/T_r - 1/T)/R - 17.56536(T_r/T - 1 + \ln(T/T_r))/R + 0.6449885(T_r(T_r/T - 1) + T - T_r)/2R - 0.0020876305(2T_r^2(T_r/T - 1) + T^2 - T_r^2)/6R - 6.915704 \times 10^{-7}(3T_r^3(T_r/T - 1) + T^3 - T_r^3)/12R - 0.00637407(1.5T_r^{1.5}(T_r/T - 1) + T^{1.5} - T_r^{1.5})/3.75R \quad \text{(A6)}$$

where T_r is equal to 254.63 K. Deviations of all data from the fitted equation are shown in Figure 14.

Partial pressure products $pHNO_3 \cdot pH_2O$ above nitric acid monohydrate (NAM) have been determined by Hanson and Mauersberger[9,23] and by Worsnop et al.[22] Values from the fitted equations given in these studies are plotted in Figure 15, together with values calculated from the solid-phase solubilities of Kuster and Kremen[18] and Pickering,[19] and aqueous phase activities and partial pressures calculated as before. The data are consistent at the higher temperatures, but there is disagreement by up to a factor of 2 at 190 K. Forsythe and Giauque[20] have determined a melting point of 235.48 K for NAM and have also measured the heat capacity of the solid. For a molality of 55.508681 mol kg^{-1} (1:1 HNO_3:H_2O) we calculate $\ln(K_P[\mathrm{NAM}])$ equal to −21.180 at 235.48 K. As was the case for the trihydrate, an expression for the $\Delta_r C_p$ terms in the equation for $\ln(K_P[\mathrm{NAM}])$ was derived, enabling the data to be compared in terms of $\Delta_r H°$ at the melting point. This is shown in Figure 16. Agreement is satisfactory, with no overall trend with temperature apparent. Data were then fitted simultaneously, yielding $\Delta_r H° = 120.82 \pm 0.15$ kJ mol^{-1} at 235.48 K and the following expression for $\ln(K_P[\mathrm{NAM}])$:

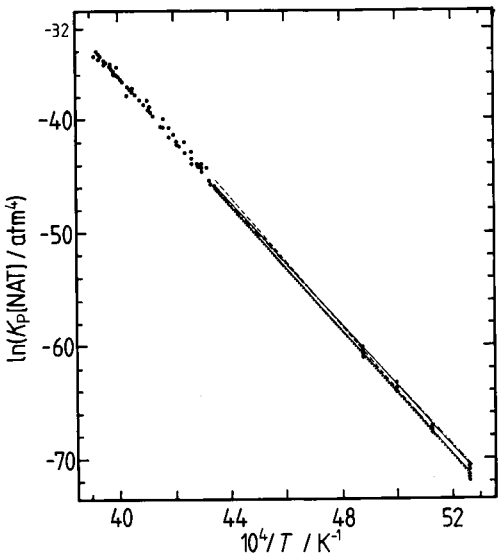

Figure 12. Equilibrium partial pressure products K_P above $HNO_3 \cdot 3H_2O_{(cr)}$ (NAT). Symbols: calculated from measurements of NAT saturation in aqueous HNO_3[18,19] and the revised thermodynamic model of Clegg and Brimblecombe (see Appendix I), or from $pHNO_3$ and pH_2O determined directly above solutions saturated with respect to NAT.[9,23] Lines: fitted equations from sources listed in Table 4.

$$\ln(K_P[\mathrm{NAM}]) = -21.180 + 120.82 \times 10^3(1/T_r - 1/T)/R + 55.824653(T_r/T - 1 + \ln(T/T_r))/R - 0.4827521(T_r(T_r/T - 1) + T - T_r)/2R + 0.0012382255(2T_r^2(T_r/T - 1) + T^2 - T_r^2)/6R - 6.915704 \times 10^{-7}(3T_r^3(T_r/T - 1) + T^3 - T_r^3)/12R - 0.00212469(1.5T_r^{1.5}(T_r/T - 1) + T^{1.5} - T_r^{1.5})/3.75R \quad \text{(A7)}$$

where T_r is equal to 235.48 K. Deviations of all data from the fitted equation are shown in Figure 17.

Ji and Petit[24] have investigated calorimetrically the formation of nitric acid dihydrate (NAD) in aqueous solution, and present the freezing curve in their Figure 9 for ∼230.5 K to ∼235.7 K. Partial pressure products of HNO_3 and H_2O over the solid have been determined by Worsnop et al.[22] and Fox et al.[25] from about 189−215 K, with a few additional measurements by Hanson and Ravishankara.[26]

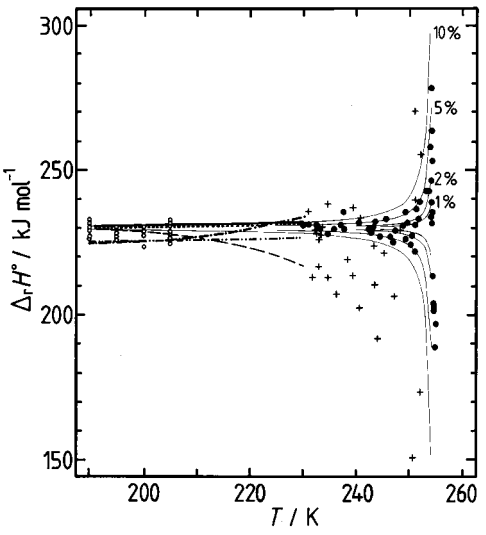

Figure 13. The enthalpy change ($\Delta_r H°$) for the solid ⇌ vapor equilibrium of $HNO_3 \cdot 3H_2O_{(cr)}$ (NAT), calculated from experimentally derived vapor pressure products K_P. Symbols: (dot) from data for NAT saturation in aqueous HNO_3[18,19] and the revised thermodynamic model of Clegg and Brimblecombe (see Appendix I), (cross) Hanson and Mauersberger[9] for aqueous solutions saturated with respect to NAT (their Figure 3), (open circle) Hanson and Mauersberger[23] for solid NAT at four temperatures (their Figure 1). Lines: (solid) Hanson and Mauersberger[23] for the NAT/NAM boundary, (dash/dot) Hanson and Mauersberger[9] for the NAT/NAM boundary, (dash/double dot) Hanson and Mauersberger[9] for the NAT/ice boundary, but using pH_2O over ice calculated using the equation of Clegg and Brimblecombe,[4] (dashed) Worsnop et al.[22] for solid NAT, (dotted) Hanson and Mauersberger[23] for the NAT/ice boundary, but using pH_2O over ice calculated using the equation of Clegg and Brimblecombe.[4] Fine solid lines indicate the change in $\Delta_r H°$ caused by errors in K_P of 1%, 2%, 5%, and 10% (marked). Note the steep increase as the melting point is approached.

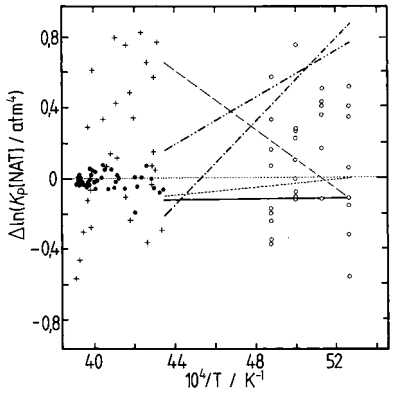

Figure 14. Deviations of the fitted equation for $\ln(K_P[NAT])$ (eq A6) from experimentally derived values. Symbols: (dot) from data for NAT saturation in aqueous HNO_3[18,19] and the revised thermodynamic model of Clegg and Brimblecombe (Appendix I), (cross) Hanson and Mauersberger[9] for aqueous solutions saturated with respect to NAT (their Figure 3), (open circle) Hanson and Mauersberger[23] for solid NAT at four temperatures (their Figure 1). Lines: (solid) Hanson and Mauersberger[23] for the NAT/NAM boundary, (dash/dot) Hanson and Mauersberger[9] for the NAT/NAM boundary, (dash/double dot) Hanson and Mauersberger[9] for the NAT/ice boundary, using pH_2O over ice calculated using the equation of Clegg and Brimblecombe,[4] (dashed) Worsnop et al.[22] for solid NAT, (dotted) Hanson and Mauersberger[23] for the NAT/ice boundary, using pH_2O over ice calculated using the equation of Clegg and Brimblecombe.[4]

Calculated K_P from the solubilities of Ji and Petit,[24] and values from Fox et al.[25] (their Figure 4) and Hanson and Ravishankara[26] (their Figure 1) were found to be consistent with one another.

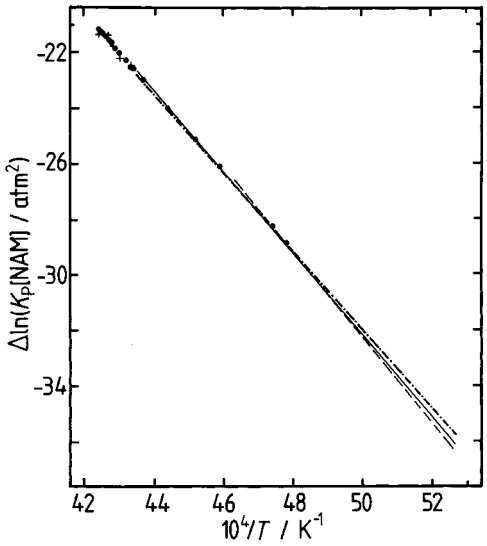

Figure 15. Equilibrium partial pressure products K_P above $HNO_3 \cdot H_2O_{(cr)}$ (NAM). Symbols: (dot) calculated measurements of NAM saturation in aqueous HNO_3[18,19] and the revised thermodynamic model of Clegg and Brimblecombe (see Appendix I), (plus) from $pHNO_3$ and pH_2O directly determined above solutions saturated with respect to NAM.[9,23] Lines: (solid) Hanson and Mauersberger[23] for the NAT/NAM boundary, (dash/dot) Hanson and Mauersberger[9] for the NAT/NAM boundary, (dash) Worsnop et al.[22] for solid NAM.

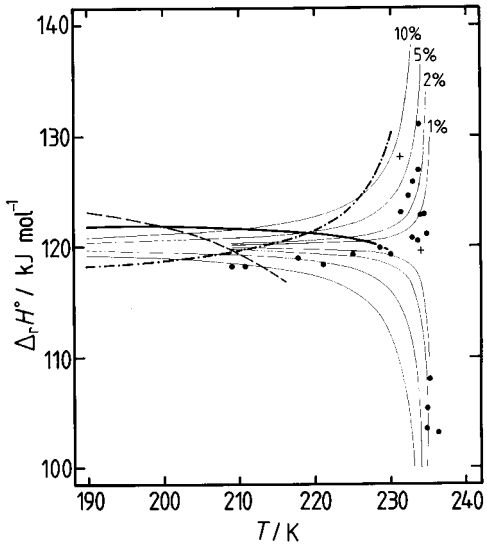

Figure 16. The enthalpy change ($\Delta_r H°$) for the solid ⇌ vapor equilibrium of $HNO_3 \cdot H_2O_{(cr)}$ (NAM), calculated from experimentally derived vapor pressure products K_P. Symbols: (dot) calculated from measurements of NAM saturation in aqueous HNO_3[18,19] and the revised thermodynamic model of Clegg and Brimblecombe (see Appendix I), (plus) from $pHNO_3$ and pH_2O directly determined above solutions saturated with respect to NAM[9,23] (most points are off-scale and omitted). Lines: (solid) Hanson and Mauersberger[23] for the NAT/NAM boundary, (dash/dot) Hanson and Mauersberger[9] for the NAT/NAM boundary, (dash) Worsnop et al.[22] for solid NAM. Fine solid lines indicate the change in $\Delta_r H°$ caused by errors in K_P of 1%, 2%, 5%, and 10% (marked). Note the steep increase as the melting point is approached.

The results of Worsnop et al.[22] agree with the other data at the lowest temperatures measured (<200 K), but show significant deviations at higher temperatures. Using an estimated melting temperature of 235.34 K, and $\Delta_r C_p$ terms in eq A5 calculated assuming a heat capacity of solid NAD equal to the average of NAT and NAM, the data were fitted to obtain the following expression for $\ln(K_P[NAD])$:

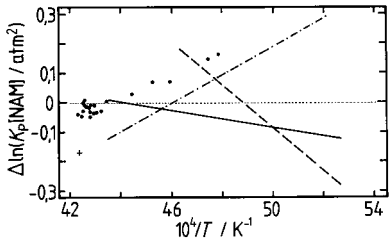

Figure 17. Deviations of the fitted equation for ln(K_P[NAM]) (eq A7) from experimentally derived values. Symbols: (dot) calculated from NAM saturation concentrations in aqueous HNO_3[18,19] and the revised thermodynamic model of Clegg and Brimblecombe (see Appendix I), (plus) from $p$$HNO_3$ and $p$$H_2O$ directly determined above solutions saturated with respect to NAM[9] (most points are off-scale and omitted). Lines: (solid) Hanson and Mauersberger[23] for the NAT/NAM boundary, (dash/dot) Hanson and Mauersberger[9] for the NAT/NAM boundary, (dash) Worsnop et al.[22] for solid NAM.

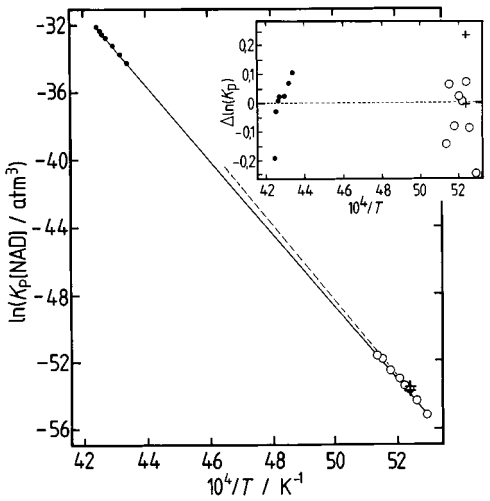

Figure 18. The equilibrium partial pressure product of HNO_3·$2H_2O$ (K_P[NAD]). Symbols: (dot) derived from the measurements of Ji and Petit[24] and the revised thermodynamic model of Clegg and Brimblecombe (see Appendix I), (open circle) Fox et al.,[25] (plus) Hanson and Ravishankara.[26] Lines: (solid) eq A8, (dashed) equation of Worsnop et al.[22]

$$\ln(K_P[\mathrm{NAD}]) = -32.2650 + 181.0 \times 10^3(1/T_r - 1/T)/R + 19.12965(T_r/T - 1 + \ln(T/T_r))/R + 0.0811182(T_r(T_r/T - 1) + T - T_r)/2R - 0.0004247025(2T_r^2(T_r/T - 1) + T^2 - T_r^2)/6R - 6.915704 \times 10^{-7}(3T_r^3(T_r/T - 1) + T^3 - T_r^3)/12R - 0.00424938(1.5T_r^{1.5}(T_r/T - 1) + T^{1.5} - T_r^{1.5})/3.75R \quad \text{(A8)}$$

where T_r is equal to 235.34 K. The data and fitted model are shown in Figure 18, together with predictions from the equation of Worsnop et al.[22]

Although Carslaw et al.[2] did not present equilibrium constants K_P for the HNO_3 hydrates, these are implicit in their results and can be calculated using eq 7. In Figure 19 we compare their effective K_P with the fitted values determined here. Differences are mostly less than 10%, which is similar or lower than the uncertainty in the partial pressure product data shown above.

The Solubility Constant (^xK_S) of HNO_3·$2H_2O_{(cr)}$. Values of ^xK_S(NAD) consistent with the expression for K_P(NAD) given above can be calculated using eq 7, the expression for ^xK_H(HNO_3) in Appendix I and $p$$H_2O$° as given by Clegg and Brimblecombe.[4] However, the model of Carslaw et al.[2] must

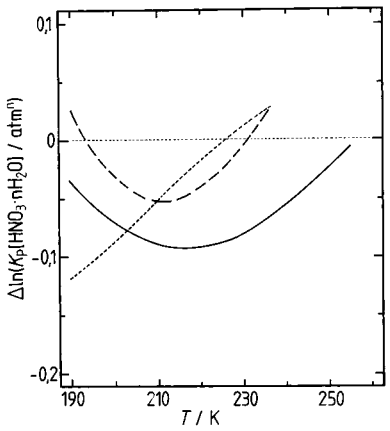

Figure 19. Comparison of equilibrium partial pressure products K_P over the nitric acid hydrates, showing the difference between ln(K_P-[HNO_3·nH_2O]) calculated using the model of Carslaw et al.[2] and eqs A6−A8 in this work. Lines: (solid) HNO_3·$3H_2O_{(cr)}$, (dashed) HNO_3·$2H_2O_{(cr)}$, (dotted) HNO_3·$H_2O_{(cr)}$. (Δln(K_P) is positive where the model of Carslaw et al.[2] yields a higher partial pressure product.)

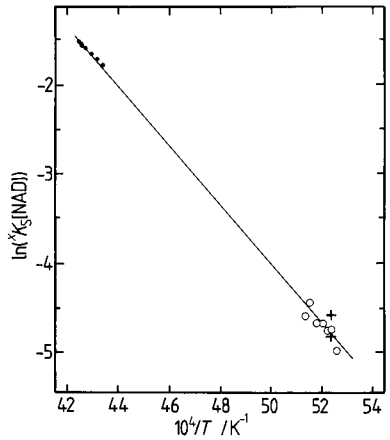

Figure 20. The activity product of HNO_3·$2H_2O$ (^xK_S[NAD]). Symbols: (dot) Ji and Petit,[24] (open circle) Fox et al.,[25] (plus) Hanson and Ravishankara.[26] Line: eq A9. See text for details of how the saturated solution compositions (Ji and Petit[24]), and partial pressures or partial pressure products (Fox et al.,[25] Hanson and Ravishankara[26]) were used to obtain ^xK_S.

be used to predict H^+ and NO_3^- activities for calculations of equilibrium NAD formation in solution mixtures. To ensure consistency, we have calculated ^xK_S(NAD) directly from the solubilities of Ji and Petit[24] using the model, and also from measured K_P of Fox et al.,[25] and $p$$HNO_3$ and $p$$H_2O$ of Hanson and Ravishankara,[26] using eq 4 above and eq 20 of Carslaw et al.[2] These values of ^xK_S were then fitted as a function of temperature yielding:

$$\ln(^xK_S[\mathrm{NAD}]) = (12.59 \pm 0.22) - (3320.2 \pm 45)/T \quad \text{(A9)}$$

The result is shown in Figure 20. A part of the calculated freezing curve of aqueous HNO_3, including the formation of NAD, is plotted in Figure 21.

Appendix III

Model Revisions and Comparisons with Recent Data. In this appendix partial pressures of HCl and HNO_3 predicted using the model of Carslaw et al.[2] are compared with recent measurements, and the model is also revised for the calculation of activity coefficients and solubilities of HBr in aqueous H_2SO_4.

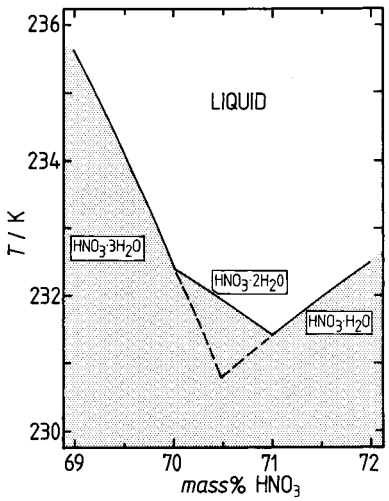

Figure 21. Calculated solid/liquid phase diagram of aqueous HNO_3, showing the formation of nitric acid dihydrate.

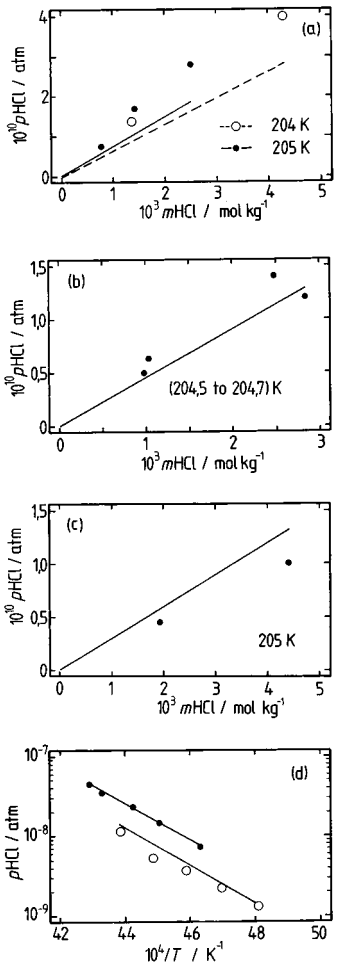

Figure 22. Equilibrium partial pressures of HCl (pHCl) above HCl−HNO_3−H_2SO_4−H_2O mixtures at low temperature. Symbols: data of Hanson[13] (plots a−c), and Elrod et al.[12] (plot d). Lines: model of Carslaw et al.[2] (a) $mH_2SO_4 = 7.69$ mol kg^{-1}, $mHNO_3 = 2.39$ mol kg^{-1}; (b) $mH_2SO_4 = 5.75$ mol kg^{-1}, $mHNO_3 = 5.01$ mol kg^{-1}; (c) $mH_2SO_4 = 3.83$ mol kg^{-1}, $mHNO_3 = 7.51$ mol kg^{-1}; (d) (dot) 48 mass % H_2SO_4, 3.5 mass % HNO_3, and 3.9×10^{-3} mol dm^{-3} HCl; (open circle) 36.2 mass % H_2SO_4, 12.5 mass % HNO_3, 6.2×10^{-3} mol dm^{-3} HCl.

HCl−HNO_3−H_2SO_4−H_2O. Equilibrium pHCl and $p$$HNO_3$ above these mixtures have been measured by Elrod et al.[12] and by Hanson[13] (see Table 5). Predicted pHCl are compared with measured values for the compositions studied by Hanson[13] in Figure 22. There is reasonable agreement overall. Although it is difficult to draw firm conclusions from such a small data set, it may be that the predicted pHCl are too low for solutions containing mainly H_2SO_4 (Figure 22a), but too high for solutions containing mostly HNO_3 (Figure 22c). However, the measurements of Elrod et al.[12] are in generally close agreement with the calculated partial pressures (Figure 22d).

Robinson et al.[27] have recently studied the uptake of HCl by aqueous H_2SO_4 at stratospheric temperatures and determined

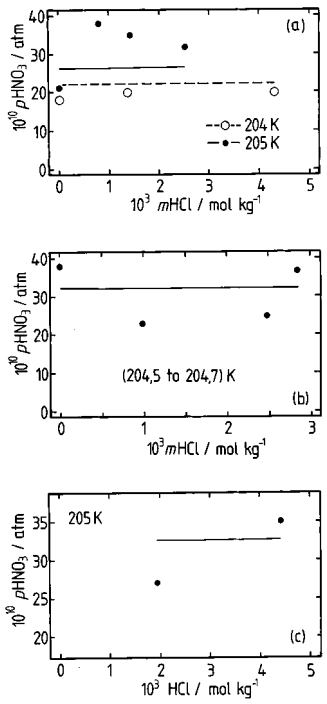

Figure 23. Equilibrium partial pressures of HNO_3 above HCl−HNO_3−H_2SO_4−H_2O mixtures at low temperature. Symbols: data of Hanson.[13] Lines: model of Carslaw et al.[2] (a) $mH_2SO_4 = 7.69$ mol kg^{-1}, $mHNO_3 = 2.39$ mol kg^{-1}; (b) $mH_2SO_4 = 5.75$ mol kg^{-1}, $mHNO_3 = 5.01$ mol kg^{-1}; (c) $mH_2SO_4 = 3.83$ mol kg^{-1}, $mHNO_3 = 7.51$ mol kg^{-1}.

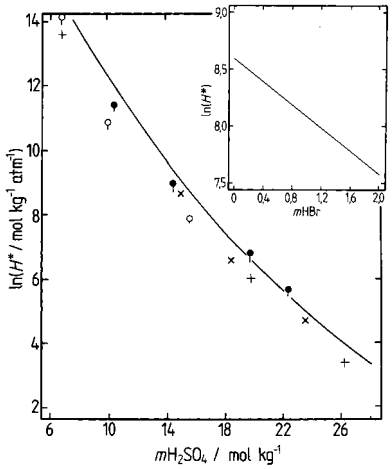

Figure 24. The effective Henry's law constant (H*) of trace HBr in aqueous H_2SO_4 at 298.15 K. Symbols: (dot) Abbatt and Nowak;[29] (open circle) Abbatt and Nowak,[29] extrapolated from measurements at low temperature; (cross) Abbatt,[30] extrapolated from measurements at low temperature; (plus) Williams et al.,[28] extrapolated from measurements at low temperature. Line: predicted values, this study. Vertical lines associated with data points from equilibrium partial pressure measurements show the extent of the (positive) correction for the HBr concentration in the test solution. The inset shows the calculated change in H* with mHBr, for a fixed H_2SO_4 molality of 15.3 mol kg^{-1} (equivalent to 60 mass % where mHBr = 0).

TABLE 5: Sources of Thermodynamic Data for HCl Partial Pressures above $HCl-HNO_3-H_2SO_4-H_2O$ Solutions at Stratospheric Temperatures

composition	data type[a]	T (K)	note	source
$HCl-HNO_3-H_2SO_4-H_2O$	pHCl	208−233	*b*	Elrod et al.[12]
$HCl-HNO_3-H_2SO_4-H_2O$	pHCl, pHNO$_3$	204−205	*c*	Hanson[13]

[a] pHCl, pHNO$_3$, equilibrium partial pressure determinations. [b] Compositions 48 mass % H_2SO_4, 3.5 mass % HNO_3, and 3.9×10^{-3} mol dm^{-3} HCl; and 36.2 mass % H_2SO_4, 12.5 mass % HNO_3, and 6.2×10^{-3} mol dm^{-3} HCl. The HCl molarities are room-temperature values and were converted to molalities assuming a solution density equal to that of H_2SO_4 at the total molarity of the solution, corrected for the difference in molar masses. [c] Compositions 20.3−44.6 mass % H_2SO_4 and 4.4−25.6 mass % HNO_3, containing $0-3.1 \times 10^{-5}$ mass fraction HCl.

TABLE 6: Sources of Thermodynamic Data for $HBr-H_2SO_4-H_2O$ Solutions

mass % H_2SO_4 min.	mass % H_2SO_4 max.	used[a]	data type[b]	T (K)	source
59.6	69.8	yes	${}^{M}H^*\sqrt{D}$[c]	200−233	Abbatt[30]
40.3	60.5	yes	pHBr[d]	218−268	Abbatt and Nowak[29]
49.5	67.6	yes	pHBr[d]	298	Abbatt and Nowak[29]
60	72	yes	${}^{M}H^*\sqrt{D}$[c]	204−240	Williams et al.[28]
54	66	yes	pHBr[e]	209−234	Williams et al.[28]
0	80	no	pHBr[f]	293−398	Gestrich et al.[31]
50	50[g]	no	pHBr[h]	205−222	Becker et al.[33]
30	72	yes	D	220−300	Klassen et al.[34]

[a] Used in the fit of the model. [b] Type of measurement: ${}^{M}H^*\sqrt{D}$, kinetic uptake data yielding the molar effective Henry's law constant (${}^{M}H^*$/mol dm^{-3} atm^{-1}) of HBr; pHBr, equilibrium partial pressure; D, diffusion coefficient of HBr in aqueous H_2SO_4. [c] Values of ${}^{M}H^*$ were obtained using diffusion coefficients of Klassen et al.,[34] and converted to molal units using densities of aqueous H_2SO_4 from Myhre et al.[35] [d] Results were presented as ${}^{M}H^*$. Concentrations of HBr in the test solutions ranged from 0.10 to 0.50 mol dm^{-3} at room temperature (personal communication, J. P. D. Abbatt). Molalities mHBr and $m$$H_2SO_4$ were estimated assuming that the mixture density was the same as that of aqueous H_2SO_4 at the same total molarity, corrected for the difference in molecular masses. Note that the values of ${}^{M}H^*$ presented by Abbatt and Nowak[29] are not adjusted for the change of solution density (hence HBr molarity) with temperature. [e] Results were presented with HBr concentrations in molar units. The test solutions were made up from stock solutions of known mass % composition, with dilution to a fixed volume (personal communication, L. R. Williams). Molalities of HBr and H_2SO_4 were estimated assuming that the mixture density was the same as that of aqueous H_2SO_4 at the same total molarity, corrected for the difference in molecular masses. [f] Results are presented as fitting equations giving both pH2O and pHBr. [g] Solutions contain 10 mass % HBr. [h] The data were not used in the fit of the model as they appear to be inconsistent with other measurements.

values of ${}^{M}H\sqrt{D}$ for (49 to 69) mass % H_2SO_4 solutions, where ${}^{M}H^*$ (mol dm^{-3} atm^{-1}) is the molar effective Henry's law constant of HCl and D the liquid-phase diffusion coefficient of HCl. Robinson et al.[27] have also compared their own measurements, and other solubility and uptake data, with predictions of ${}^{M}H^*\sqrt{D}$ using the model of Carslaw et al.[2] to calculate ${}^{M}H^*$ (see Plate 1 of Robinson et al.[27]). The calculated ${}^{M}H^*\sqrt{D}$ agree well with the measurements over several orders of magnitude, though deviations are observed for some data sets. In these cases the model generally predicts a lower equilibrium partial pressure than would be inferred from the experimental data. Robinson et al.[27] conclude that the results overall tend to confirm the model of Carslaw et al.[2] for HCl solubility in aqueous H_2SO_4.

Calculated pHNO$_3$ over the $HCl-HNO_3-H_2SO_4-H_2O$ mixtures agree satisfactorily with the data of Hanson,[13] see Figure 23. This is to be expected as the solutions contain only low molalities of HCl, and the model is parameterized for the interactions occurring in $HNO_3-H_2SO_4-H_2O$ solutions (see section IV of Carslaw et al.[2]).

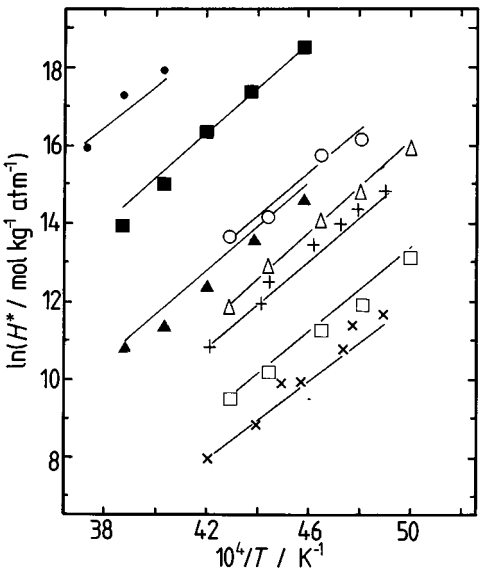

Figure 25. Effective Henry's law constants (H^*) of HBr in aqueous H_2SO_4 from both kinetic uptake and equilibrium partial pressure measurements. Symbols: (dot) 40.3 mass % H_2SO_4, (solid square) 48.8 mass % H_2SO_4, (solid triangle) 60.5 mass % H_2SO_4, (open circle) 59.6 mass % H_2SO_4, (open triangle) 64.4 mass % H_2SO_4, (open square) 69.8 mass % H_2SO_4, (plus) 66 mass % H_2SO_4, (cross) 72 mass % H_2SO_4. All solid symbols are equilibrium partial pressure data of Abbatt and Nowak,[29] open symbols are kinetic uptake data of Abbatt,[30] and the "plus" and "cross" are kinetic uptake data of Williams et al.[28] Note that measurements of Williams et al.[28] for 60 mass % H_2SO_4 are discordant with other data and are omitted. Lines: fitted values. See the notes to Table 6 for details of how the molal compositions of the solutions were estimated, and measured ${}^{M}H^*$ (mol dm^{-3} atm^{-1}) values converted to molal units.

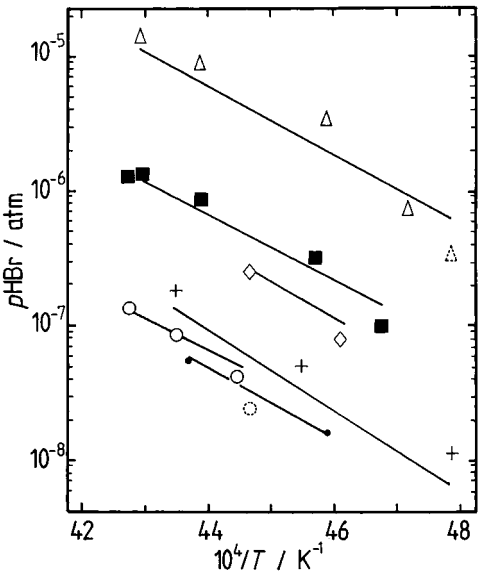

Figure 26. Equilibrium partial pressures of HBr (pHBr) above $HBr-H_2SO_4-H_2O$ mixtures. Data of Williams et al.[28] Symbols: (open triangle) 66 mass % H_2SO_4 and 0.33 mol dm^{-3} HBr, (solid square) 66 mass % H_2SO_4 and 0.05 mol dm^{-3} HBr, (open diamond) 60 mass % H_2SO_4 and 0.33 mol dm^{-3} HBr, (plus) 60 mass % H_2SO_4 and 0.05 mol dm^{-3} HBr, (open circle) 54 mass % H_2SO_4 and 0.66 mol dm^{-3} HBr, (dot) 54 mass % H_2SO_4 and 0.33 mol dm^{-3} HBr. The symbols plotted with broken outlines were not included in the fit. Lines: fitted values. See the notes to Table 6 for details of how the molal compositions of the solutions were estimated.

TABLE 7: Thermodynamic Properties of Reactants and Products in Equations 11 to 13[a]

species	$\Delta_f G°$ (kJ mol^{-1})	$\Delta_f H°$ (kJ mol^{-1})	*a*	*b*	*c*	*d*	note
$H^+_{(aq)}$	0	0	0	0	0	0	*b*
$NO_3^-{}_{(aq)}$	−108.74[c]	−205.0[c]	−568.03908	2.2990619	-2.13091×10^{-3}	0	*d*
$Cl^-{}_{(aq)}$	−131.228[c]	−167.159[c]	−514.195	1.3	0	0	*e*
$NOCl_{(aq)}$	67.16[c]	20.138[f]					
$Cl_{2(aq)}$	6.94[c]	−23.4[c]					
$H_2O_{(l)}$	−241.294[c]	−287.718[c]	295.1626	−1.540508	0.0027023	0	*g*
$HNO_{2(aq)}$	−50.6[c]	−119.2[c]					
$NO_{(aq)}$	102.133	78.819					*h*
$NO_{2(aq)}$	62.222	12.309					*i*
$Cl_{2(g)}$	0[j]	0[j]	25.85177	0.0370274	-3.31044×10^{-5}	0	*k*
$NOCl_{(g)}$	66.096[l]	51.714[l]	27.92211	0.0791387	-7.79266×10^{-5}	0	*k*
$HNO_{2(g)}$	−43.934[l]	−78.827[l]	27.04109	0.063755	0	0	*k*
$NO_{(g)}$	86.600[l]	90.291[l]	36.18087	−0.051151	1.35323×10^{-4}	-1.17403×10^{-7}	*k*
$NO_{2(g)}$	51.258[l]	33.095[l]	34.80326	−0.032165	1.87363×10^{-4}	-1.84614×10^{-7}	*k*

[a] Terms *a*-*d* give the heat capacities of the species as a function of temperature (eqs 8 and A14), where known. Partial pressures of $HCl_{(g)}$ and $HNO_{3(g)}$ were calculated using Henry's law constants from Carslaw et al.,[2] while that of $H_2O_{(g)}$ was calculated using the liquid phase water activity and vapor pressure of pure water given by Clegg and Brimblecombe.[4] [b] Defined. [c] Wagman et al.[36] [d] Heat capacity terms *a*-*d* are from Clegg and Brimblecombe.[3] [e] Heat capacity terms *a*-*d* are from Carslaw et al.[2] [f] Estimated assuming that $\Delta_r S°/R$ (the value of $\ln(K_H)$ at $1/T = 0$, where K_H is the Henry's law constant in mol kg^{-1} atm^{-1}) is equal to −13.167, as that for HOCl.[37] [g] Values of $\Delta_f G°$ and $\Delta_f H°$ are for 273.15 K (converted from 298.15 K values by integration using published heat capacity data) and therefore require the use of $T_r = 273.15$ K in eq A14. Terms *a*-*d* are from Clegg and Brimblecombe.[4] [h] These values were estimated using $\Delta_f G°$ and $\Delta_f H°$ for $NO_{(g)}$ from Chase et al.,[21] $K_H(NO) = 1.9 \times 10^{-3}$ mol kg^{-1} atm^{-1} [38] and $\Delta_r H°$ for the dissolution reaction equal to −12.472 kJ mol^{-1}.[38] [i] These values were estimated using $\Delta_f G°$ and $\Delta_f H°$ for $NO_{2(g)}$ from Chase et al.,[21] $K_H(NO_2) = 1.2 \times 10^{-2}$ mol kg^{-1} atm^{-1} [38] and an estimated $\Delta_r H°$ for the dissolution reaction equal to −20.786 kJ mol^{-1}.[39] [j] Defined. [k] Terms *a*-*d* were fitted to data tabulated by Chase et al.[21] [l] Chase et al.[21]

Reactions 11−13 should occur in these solution mixtures. For the compositions studied by Hanson[13] we calculate equilibrium partial pressures of Cl_2 up to 25 times greater than those of HCl. However, as noted in section 4.3 the reactions may be sufficiently slow that little Cl_2 is generated over the period of the experiment, which utilizes a flow tube rather than a sealed cell.

HBr−H_2SO_4−H_2O. Carslaw et al.[2] based their model upon activities and equilibrium partial pressures of HBr above pure aqueous HBr solutions at 298.15 K, with thermal properties (enthalpies and heat capacities) used to obtain the variation of the activities and Henry's law constant with temperature. Activities of HBr in aqueous H_2SO_4 solutions were estimated without parameters for the ternary interactions expected to occur in the mixtures. Comparisons with the data available at the time[28] (see Figure 14 of Carslaw et al.[2]) showed reasonable agreement with the observed trend in the effective Henry's law constant of HBr (*H**) with temperature, but quite large errors for solutions dilute with respect to H_2SO_4.

Several additional studies of HBr solubility in aqueous H_2SO_4 at low temperature have been carried out since the work of Williams et al.,[28] see Table 6, and the results have been used to revise the model of Carslaw et al.[2] First, all data were converted to molality based units, where necessary (see notes to Table 6), and checked for consistency. Figure 24 shows ln(*H**) at 298.15 K measured by Abbatt and Nowak[29] compared with extrapolations, as ln(*H**) versus 1/*T*, from the low-temperature measurements of Abbatt,[30] Abbatt and Nowak,[29] and Williams et al.[28] It is clear, first of all, that the solubility of HBr in aqueous H_2SO_4 varies strongly with H_2SO_4 concentration, for example, *H** decreases by almost a factor of 1000 from 50 mass % to 70 mass % H_2SO_4. Second, the extrapolations of the low temperature data, which are derived from both equilibrium partial pressure and kinetic uptake experiments, agree reasonably well with the *H** values determined at 298.15 K suggesting consistency of the different data sets over a wide range of temperatures. The inset to Figure 24 shows calculated *H** for a 15.3 mol kg^{-1} (60 mass%) H_2SO_4 solution as a function of added HBr. The decrease in ln(*H**) with *m*HBr is large: a value of 8.6 for trace HBr in the aqueous phase (which is appropriate for atmospheric conditions) is reduced to 8.1 for an aqueous HBr concentration of 1 mol kg^{-1}, a 39% change in *H**. Such differences need to be taken into account when interpreting *H** values from equilibrium *p*HBr measurements, as the test solutions can contain quite high molalities of HBr. Effective Henry's law constants (*H**) from the fitted model are also shown in Figure 24 and agree satisfactorily with the measured values of *H** at 298.15 K.

Measurements of *H** and *p*HBr from sources listed in Table 6 were used to determine the ion interaction parameters $W_{HSO_4,Br,H}$ and $W_{SO_4,Br,H}$, and also $\partial\Delta_r C_p/\partial T$ for the Henry's law reaction $HBr_{(g)} \rightleftharpoons H^+_{(aq)} + Br^-_{(aq)}$. The revised expression for ${}^xK_H$(HBr), and for the two interaction parameters, are given below:

$$\ln({}^xK_H[\mathrm{HBr}]) = 12.5062 - 85.13 \times 10^3(1/T_r - 1/T)/R + 348.78(T_r/T - 1 + \ln(T/T_r))/R - 1.743((T_r/T - 1)T_r + T - T_r)/2R \quad \text{(A10)}$$

$$W_{HSO_4,Br,H} = -0.798159 \quad \text{(A11)}$$

$$W_{SO_4,Br,H} = 13.6035 - 39722.2(1/T_r - 1/T) \quad \text{(A12)}$$

where T_r is equal to 298.15 K. Carslaw et al.[2] assumed a value of $\partial\Delta_r C_p/\partial T = 1.3$ J mol^{-1} K^{-2} for the dissolution reaction, the same as that for HCl. The value of −1.743 J mol^{-1} K^{-2} obtained here is of similar magnitude. However, the estimate should be treated with caution as it has been obtained only indirectly, from an optimization of solubilities in concentrated solutions, rather than from calorimetric data. Values of ${}^xK_H$(HBr) calculated from eq A10 above are greater than those given by Carslaw et al.[2] by about 10% at 250 K, 67% at 220 K, and by a factor of 4 at 190 K.

Measured and fitted values of *H**(HBr), and equilibrium partial pressures *p*HBr, are shown in Figures 25 and 26 for HBr−H_2SO_4−H_2O solutions at low temperature. (Note that data of Williams et al.[2] for 60 mass% H_2SO_4 solutions were omitted as these appear to be discordant with other measurements.) The solubilities and partial pressures cover the temperature range

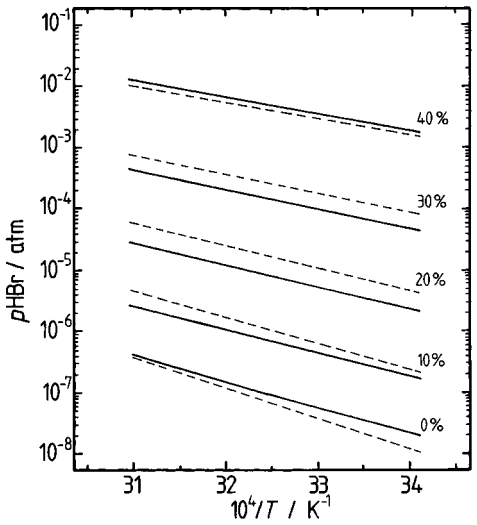

Figure 27. Comparison of calculated equilibrium partial pressures of HBr (*p*HBr) above aqueous solutions containing 20 mass % HBr and (0−40) mass % H_2SO_4 (indicated on the graph). Lines: (solid) this study, (dashed) equation of Gestrich et al.[31]

200−298.15 K, and H_2SO_4 concentrations 40−72 mass %, and the model agrees well with the data overall.

In Figure 27 equilibrium *p*HBr calculated from the equations of Gestrich et al.[31] are compared with the model, for 20 mass % HBr and 0−40 mass % H_2SO_4, from 293.15−323.15 K. The work of Gestrich et al.[31] appears to be based upon studies carried out at high temperature and concentration, and agreement is relatively poor. This is true even for pure aqueous HBr, for which *p*HBr from the equations of Gestrich et al.[31] are lower than predicted by a factor of 2 at 293.15 K, and by about 50% at 298.15 K. For this composition and temperature the present model is well constrained by activity and partial pressure data and is likely to be accurate to within a few percent. The fact that there is improved agreement at higher temperatures for pure aqueous HBr, and higher H_2SO_4 concentrations generally, may reflect the composition and temperature ranges fitted by Gestrich et al.[31] rather than real inconsistencies between the models or the data upon which they are based.

Appendix IV

Calculating the Equilibrium Constants for Reactions 11−13. The equilibrium constants *K* were calculated from the usual formula:

$$\ln(K) = -\Delta_r G^\circ/RT \qquad \text{(A13)}$$

where $\Delta_r G^\circ$ is the Gibbs energy change for the reaction ($\Sigma_{products} - \Sigma_{reactants}$) at temperature *T*. The value of G° for each chemical species is given by:

$$\begin{aligned} G^\circ = \Delta_f G^\circ(T/T_r) - RT(\Delta_f H^\circ(1/T_r - 1/T)/R + \\ a(T_r/T - 1 + \ln(T/T_r))/R + \\ b(T_r(T_r/T - 1) + T - T_r)/2R + \\ c(2T_r^2(T_r/T - 1) + T^2 - T_r^2)/6R + \\ d(3T_r^3(T_r/T - 1) + T^3 - T_r^3)/12R) \end{aligned} \qquad \text{(A14)}$$

where $\Delta_f G^\circ$(J mol^{-1}) is the Gibbs energy of formation at reference temperature T_r (here 298.15 K), $\Delta_f H^\circ$ (J mol^{-1}) is the enthalpy of formation (also at T_r), and the heat capacity, C_p, is given as a function of temperature by: $C_p = a + bT + cT^2 + dT^3$. Values of $\Delta_f G^\circ$, $\Delta_f H^\circ$, and constants *a*−*d* for each of the species in reactions 11−13 are listed in Table 7. Note that heat capacities for many of the aqueous species (Cl_2, NOCl, NO, NO_2, and HNO_2) are not known. For simplicity, the heat capacities of the gas-phase molecules were set to zero when calculating their Henry's law constants, making $\ln(K_H)$ proportional to $1/T$.

References and Notes

(1) Carslaw, K. S.; Peter, Th.; Clegg, S. L. *Rev. Geophys.* **1997**, *35*, 125−154.
(2) Carslaw, K. S.; Clegg, S. L.; Brimblecombe, P. *J. Phys. Chem.* **1995**, *99*, 11557−11574.
(3) Clegg, S. L.; Brimblecombe, P. *J. Phys. Chem.* **1990**, *94*, 5369−5380; *J. Phys. Chem.* **1992**, *96*, 6854.
(4) Clegg, S. L.; Brimblecombe, P. *J. Chem. Eng. Data* **1995**, *40*, 43−64.
(5) Mellor, J. W. *A Comprehensive Treatise on Inorganic and Theoretical Chemistry*; Longmans, Green and Co.: London, 1928; Vol. VIII, pp 612−624.
(6) Clegg, S. L.; Pitzer, K. S.; Brimblecombe, P. *J. Phys. Chem.* **1992**, *96*, 9470−9479; *J. Phys. Chem.* **1994**, *98*, 1368; *J. Phys. Chem.* **1995**, *99*, 6755.
(7) Massucci, M.; Clegg, S. L.; Brimblecombe, P. *J. Chem. Eng. Data* **1996**, *41*, 765−778.
(8) Where possible, tabulated values (Vacuum Generators, Maunsell Rd., Hastings, U.K.) of the relative sensitivity of the quadrupole mass spectrometer to the components under investigation were used. For HCl this value was checked by comparing the signals due to HCl and H_2O during determination of the total pressure above the more concentrated HCl solution, at the highest temperatures measured (for which the relative amount of HCl to H_2O in the vapor was greatest, see inset of Figure 5). Both measured partial pressures (based on the sensitivities referred to above) and the measured total pressure (from the capacitance gauges) agreed well with values calculated using the model of Carslaw et al.[2] The relative sensitivity of the instrument for HNO_3 had to be estimated. This was done using the quadrupole mass spectrometer signals due to HNO_3 and H_2O recorded during total pressure measurements of the 15.73 mol kg^{-1} HNO_3 solution, for a temperature of about 293 K. Under these conditions, for which the model is known to be reliable,[3] measured total pressures (from the capacitance gauge) agreed well with predictions. The model was then used to calculate the partial pressures, from which the relative sensititivity was determined.
(9) Hanson, D.; Mauersberger, K. *J. Phys. Chem.* **1988**, *92*, 6167−6170.
(10) Miller, E. *J. Chem. Eng. Data* **1983**, *28*, 363−367.
(11) Oishi, Y. *J. Chem. Soc. Jpn.* **1950**, *53*, 418−420.
(12) Elrod, M. J.; Koch, R. E.; Kim, J. E.; Molina, M. J. *Faraday Discuss.* **1995**, *100*, 269−278.
(13) Hanson, D. R. *J. Phys. Chem.* **1998**, *102*, 4794−4807.
(14) Dye, J. E.; Baumgardner, D.; Gandrud, B. W.; Kawa, S. R.; Kelly, K. K.; Loewenstein, M.; Ferry, G. V.; Chan, K. R.; Gary, B. L. *J. Geophys. Res.* **1992**, *97*, 8015−8034.
(15) Carslaw, K. S.; Luo, B. P.; Clegg, S. L.; Peter, Th.; Brimblecombe, P.; Crutzen, P. *J. Geophys. Res. Lett.* **1994**, *21*, 2479−2482.
(16) Hovey, J. K.; Hepler, L. G. *Can. J. Chem.* **1989**, *67*, 1489−1495.
(17) Mischenko, K. P. *Landolt-Bornstein Physikalische-Chemische Tabellen*, 5. 2nd Supplement; J. Springer: Berlin, 1931; Vol. 5, p 1657.
(18) Kuster, F. W.; Kremann, R. Z. *Z. Anorg. Chem.* **1904**, *41*, 1−42.
(19) Pickering, S. U. *J. Chem. Soc.* **1893**, *63*, 436−443.
(20) Forsythe, W. R.; Giauque, W. F. *J. Am. Chem. Soc.* **1942**, *64*, 48−61.
(21) Chase, M. W.; Davies, C. A.; Downey, J. R.; Frurip, D. J.; McDonald, R. A.; Syverud, A. N. *J. Phys. Chem. Ref. Data* **1985**, *14*, 1−1856.
(22) Worsnop, D. R.; Fox, L. E.; Zahniser, M. S.; Wofsy, S. C. *Science* **1993**, *259*, 71−74.
(23) Hanson, D.; Mauersberger, K. *Geophys. Res. Lett.* **1988**, *15*, 855−858.
(24) Ji, K.; Petit, J. C. *Comptes Rendus*, Ser. II, **1993**, *316*, 1743−1748.
(25) Fox, L. E.; Worsnop, D. R.; Zahniser, M. S.; Wofsy, S. C. *Science* **1995**, *267*, 351−355.
(26) Hanson, D. R.; Ravishankara, A. R. *J. Geophys. Res.* **1993**, *98*, 22931−22936.
(27) Robinson, G. N.; Worsnop, D. R.; Jayne, J. T.; Kolb, C. E. *J. Geophys. Res.* **1998**, *103*, 25371−25381.
(28) Williams, L. R.; Golden, D. M.; Huestis, D. L. *J. Geophys. Res.* **1995**, *100*, 7329−7335.
(29) Abbatt, J. P. D.; Nowak, J. B. *J. Phys. Chem.* **1997**, *101*, 2131−2137.

(30) Abbatt, J. P. D. *J. Geophys. Res.* **1995**, *100*, 14009−14017.
(31) Gestrich, W.; Kottek, C.; Van Velzen, D.; Langenkamp, H. *Chem. Ing. Technol.* **1984**, *56*, 252−253.
(32) Pickering, S. U. *J. Chem. Soc.* **1893**, *63*, 436−443.
(33) Becker, K. H.; Schrey, G.; Zabel, F. Laboratory studies of stratospheric reactions on surfaces. Report 01 LO 9104/2; Bergische University: Wuppertal, 1995.
(34) Klassen, J. K.; Hu, Z.; Williams, L. R. *J. Geophys. Res.* **1998**, *103*, 16197−16202.
(35) Myhre, C. E. L.; Nielsen, C. J.; Saastad, O. W. *J. Chem. Eng. Data* **1998**, *43*, 617−622.
(36) Wagman, D. D.; Evans, W. H.; Parker, V. B.; Schumm, I. H.; Bailey, S. M.; Churney, K. L.; Nuttall, R. L. *J. Phys. Chem. Ref. Data* **1982**, *11*, 1−392.
(37) Huthwelker, T.; Clegg, S. L.; Peter, Th.; Carslaw, K.; Luo, B. P.; Brimblecombe, P. *J. Atmos. Chem.* **1995**, *21*, 81−95.
(38) Schwartz, S. E.; White, W. H., In: *Advances in Environmental Science and Engineering*; Pfafflin, J. R., Ziegler, E. N., Eds.; Gordon and Breach: New York, 1981; Vol. 4, pp 1−45.
(39) Chameides, W. L. *J. Geophys. Res.* **1986**, *91*, 14571−14572.
(40) Wooldridge, P. J.; Zhang, R.; Molina, M. J. *J. Geophys. Res.* **1995**, *100*, 1389−1396.